nature communications

Article

https://doi.org/10.1038/s41467-025-60825-y

Large-scale synaptic dynamics drive the reconstruction of binocular circuits in mouse visual cortex

Received: 10 November 2024

Accepted: 3 June 2025

Published online: 01 July 2025

Check for updates

Katya Tsimring[1], Kyle R. Jenks[2], Claudia Cusseddu[3], Greggory R. Heller[1], Jacque Pak Kan Ip[2,4], Julijana Gjorgjieva[3] & Mriganka Sur[1,2]

In the binocular primary visual cortex, visual experience shapes neuronal responses to the contralateral and ipsilateral eye during a critical period in postnatal development. The synaptic changes that underlie the construction of binocular circuits are unknown. Using chronic in vivo two-photon imaging to record the somata and excitatory synaptic inputs onto dendritic spines of identified layer 2/3 neurons in mouse binocular visual cortex, we report that spines experience significant turnover and eye-specific remapping of their visual responses during the critical period. Spine retention is strongly linked to their calcium activity, particularly in response to the soma's preferred visual stimulus. Furthermore, spine responses become more correlated to those of their neighbors after development. Using a single-neuron model, we show that Hebbian and heterosynaptic mechanisms plausibly underlie the retention and localized organization of synaptic inputs. Our results underscore the profound dynamics at individual synapses and the fundamental synaptic mechanisms that shape the development of visual cortical neurons.

The postnatal development of neural circuits in the primary visual cortex (V1) of mammals progresses through distinct stages, driven by both intrinsic, genetically-encoded patterning and extrinsic, experience-dependent synaptic modifications[1]. Prior to eye-opening, molecular signals and spontaneous activity guide the innervation, formation, and pruning of thalamic axons onto layer 4 neurons, establishing a topographic map in V1[2–4]. At around the time of eye-opening, V1 neurons begin to exhibit orientation-selective and binocular responses[5–8], which are two emergent properties unique to V1 circuits that are further shaped by visual experience during a critical period in development[7]. While experience-dependent synaptic modifications have long been assumed to drive changes in neuronal responses[9–11], the precise nature of circuit reorganization during this critical period remains unclear.

Our understanding of how synapses are modified during the V1 critical period largely stems from visual deprivation experiments. Building upon early pioneering studies in kittens[12], careful measurements in mice show that closing one eye for a brief duration (~3 days) during a critical period spanning p21-35, with peak sensitivity at ~p28, leads to severe reduction in responses of binocular V1 (bV1) neurons to the deprived eye[13], followed by an increase in responses to the non-deprived eye (~7 days)[14]. The mechanisms underlying this ocular dominance plasticity have been extensively studied, and include changes in gene and protein expression in V1 neurons as well as structural changes in thalamocortical and intracortical axons[15–18]. Additionally, V1 neurons experience increased motility and loss of their dendritic spines[19–24], reflecting direct structural correlates of synaptic changes.

While the critical period has thus far been largely defined by the impact of monocular deprivation on bV1 responses, its role in normal development, as a period of heightened plasticity driven by visual experience, has also been increasingly clarified. The preferred orientation of binocular bV1 cells (as measured through the two eyes) is mismatched at the beginning of the critical period, but becomes more

[1]Department of Brain and Cognitive Sciences, Massachusetts Institute of Technology, Cambridge, MA, USA. [2]The Picower Institute for Learning and Memory, Massachusetts Institute of Technology, Cambridge, MA, USA. [3]School of Life Sciences, Technical University of Munich, Freising, Germany. [4]School of Biomedical Sciences, Gerald Choa Neuroscience Institute, The Chinese University of Hong Kong, Hong Kong SAR, China. e-mail: msur@mit.edu

aligned and adult-like by the end[25]. Visual deprivation during this period blocks the binocular matching of orientation preference[26]. Thus, an important function of experience-dependent development is to establish matched binocular responses in bV1 neurons. Based on these studies, which relied on measuring responses of separate neuronal populations at discrete time points, the underlying mechanism of binocular matching has been hypothesized to be the gradual alignment of thalamocortical and intracortical inputs conveying eye-specific information to binocular bV1 neurons[1,25,27]. In contrast, longitudinally tracking the responses of layer (L) 2/3 bV1 neurons through the critical period suggests an alternative view of how circuits are reorganized by visual experience[28]. Instead of showing gradual refinement of existing binocular neurons, poorly tuned and mismatched binocular neurons lose responsiveness to one eye and become monocular, whereas well-tuned monocular neurons gain input from the opposite eye, becoming binocular. Thus, the role of visual experience is seemingly to reconstruct circuits rather than refine existing binocular circuits[29].

While the refinement versus reconstruction of bV1 neuronal responses remains an active area of investigation, much less is known about how synaptic inputs onto dendritic spines of cortical neurons change and reorganize over normal development. Dendritic spines imaged in superficial layers of V1 are more motile and experience more turnover during the critical period than in adulthood[19,30], but it is unclear if this structural instability results in changes in visually driven input. Large scale loss and addition of spines during the critical period, coupled with major changes in their visually driven responses, would support the hypothesis that visual experience reconstructs rather than gradually alters the circuits that create binocular responses in bV1 neurons.

To distinguish between these hypotheses, we chronically tracked synaptic inputs to individual L2/3 bV1 neurons during the critical period (~ p22 to ~p32) using two-photon calcium imaging of somata and their dendritic spines responding to monocular and binocular viewing of visual stimuli. We found that changes in the visual responses of imaged neurons were associated with significant turnover of dendritic spines, with only 40% of spines being retained through the critical period, as well as large shifts in the monocular and binocular responses of retained spines. The fate of a spine was strongly related to its activity during binocular viewing, as spines that were retained exhibited higher levels of activity than those that were lost or added, particularly when viewing the soma's preferred stimulus. We also found that the correlation in trial-to-trial activity among neighboring spine pairs increased over development. To investigate the mechanisms that contribute to spine turnover during the critical period, we built a computational single-neuron model in which the strength of synapses changed based on the correlation between pre- and postsynaptic responses (Hebbian plasticity) and between neighboring synapses (heterosynaptic plasticity)[31–33]. We found that both mechanisms contributed to the retention of active synapses aligned to the soma, similar to our findings in vivo, and that heterosynaptic plasticity was required for increasing the clustering between co-active spine pairs.

By revealing the profound structural and functional dynamics of dendritic spines, our work supports the hypothesis that visual experience reconstructs rather than gradually alters bV1 circuits. Furthermore, it highlights the putative contributions of plasticity mechanisms to the retention and localized organization of spines, which together lead to the creation of adult-like binocular visual responses in the somata of layer 2/3 neurons during the critical period.

Results

Dendritic spines undergo structural and functional dynamics during the critical period

To examine how the functional and structural properties of dendritic spines on mouse L2/3 neurons in bV1 change over the critical period, we performed in vivo two-photon calcium and structural imaging using sparse viral labeling of GCaMP6s and mRuby2. Imaging began at ~p22-p24 and ended at ~p32-p34 to encompass most of the critical period (Fig. 1a). For the majority of included animals (10/15 mice), we validated that the imaged neuron(s) lay within the borders of bV1 by performing intrinsic signal imaging (Fig. 1b). During two-photon imaging, mice viewed drifting grating stimuli presented independently to each eye (contralateral (contra) or ipsilateral (ipsi) eye viewing) or presented to both eyes (binocular viewing). For each recorded cell, we serially imaged the soma and 2-4 dendritic segments from apical and/or basal dendrites, and analyzed the visual response properties from their fluorescent activity (see Supplementary Fig. 1 and Methods for details). Overall, we imaged a total of 1574 spines from 26 neurons at p22-24 (D1), 1166 spines from 23 neurons at p27-29 (D5), and 1384 spines from 24 neurons at p32-34 (D10). A substantial subset of these neurons and dendritic segments were repeatedly imaged across two or three timepoints (see Supplementary Fig. 2).

Somata and dendritic spines exhibited varying responses and preferences for stimulus direction to binocular, contra eye, or ipsi eye viewing (Fig. 1c). Neurons that were repeatedly imaged across development in some cases exhibited loss or gain in visual responses to binocular, contra eye, or ipsi eye viewing between timepoints (Fig. 1d–f). Neurons that responded to a particular viewing condition (binocular, contra, or ipsi) had a higher proportion of spines responding to the same viewing condition than neurons that were unresponsive to that condition (Fig. 1d–f insets). This suggests that the number of visually responsive inputs is a strong predicter of somatic visual responsiveness.

Given the dynamics in somatic responses we observed during the critical period, we suspected that there was also high turnover of spines, and were interested in determining how the loss and retention of spines related to their visual responses. Thus, we chronically tracked the fate of 793 dendritic spines on 14 neurons every 5 days (D1, D5, and D10), starting at p22-24 (Fig. 2a). In some of our analyses, we also included neurons that were tracked for only two timepoints (D1 to D5 or D5 to D10).

While the average spine density and size was consistent across the 10-day period (Supplementary Fig. 3), there was significant turnover of spines between timepoints. 32% of spines imaged on D1 had been lost by D5, while 24% of spines imaged on D5 were newly added. From D5 to D10, the rate of spine elimination and addition remained consistent with 27% of spines lost and 24% added (Fig. 2b). Of the spines observed at D1, only 40% (181/449) remained by D10, and half of spines that were added on D5 were subsequently lost by D10 (Fig. 2c), highlighting the transient nature of newly formed spines during the critical period.

We next examined whether a spine's fate (lost, added, or retained) could be explained by their responses to the eye-specific and binocular viewing conditions. While response type did not influence spine retainment from D1 to D5, we found that spines that responded to both the contra and ipsi eye viewing conditions, which we will be referring to as C + I spines, were more likely to be retained than unresponsive spines from D5 to D10 (Fig. 2d). We next asked whether the binocular or eye-specific responses of dendritic spines that were retained across the 10-day period remained stable. Surprisingly, responsive retained dendritic spines often lost or shifted their binocular or eye-specific responses, with 30% (12/40) of spines maintaining their binocular response from D1 to D5 to D10 (Fig. 2e) and only 11% (6/53) of spines maintaining their contra and/or ipsi response (Fig. 2f). On the other hand, 82% (96/117) of spines unresponsive to binocular viewing and 74% (79/104) of spines unresponsive to the contra or ipsi eye viewing remained unresponsive from D1 to D5 to D10. The responses of our tracked neurons were also dynamic between timepoints, and while we imaged neurons that were visually responsive on D1 (14/14 neurons responsive to any condition), the majority of the neurons we imaged became unresponsive by D10 (10/14 neurons unresponsive to any condition). These results suggest that activity unrelated to visual drive, or at least not encompassed by our stimuli, is important for the retention of many inputs.

Finally, we quantified the fraction of spines responsive to each condition (binocular, contra, or ipsi) on somas responsive to the same

https://doi.org/10.1038/s41467-025-60825-y

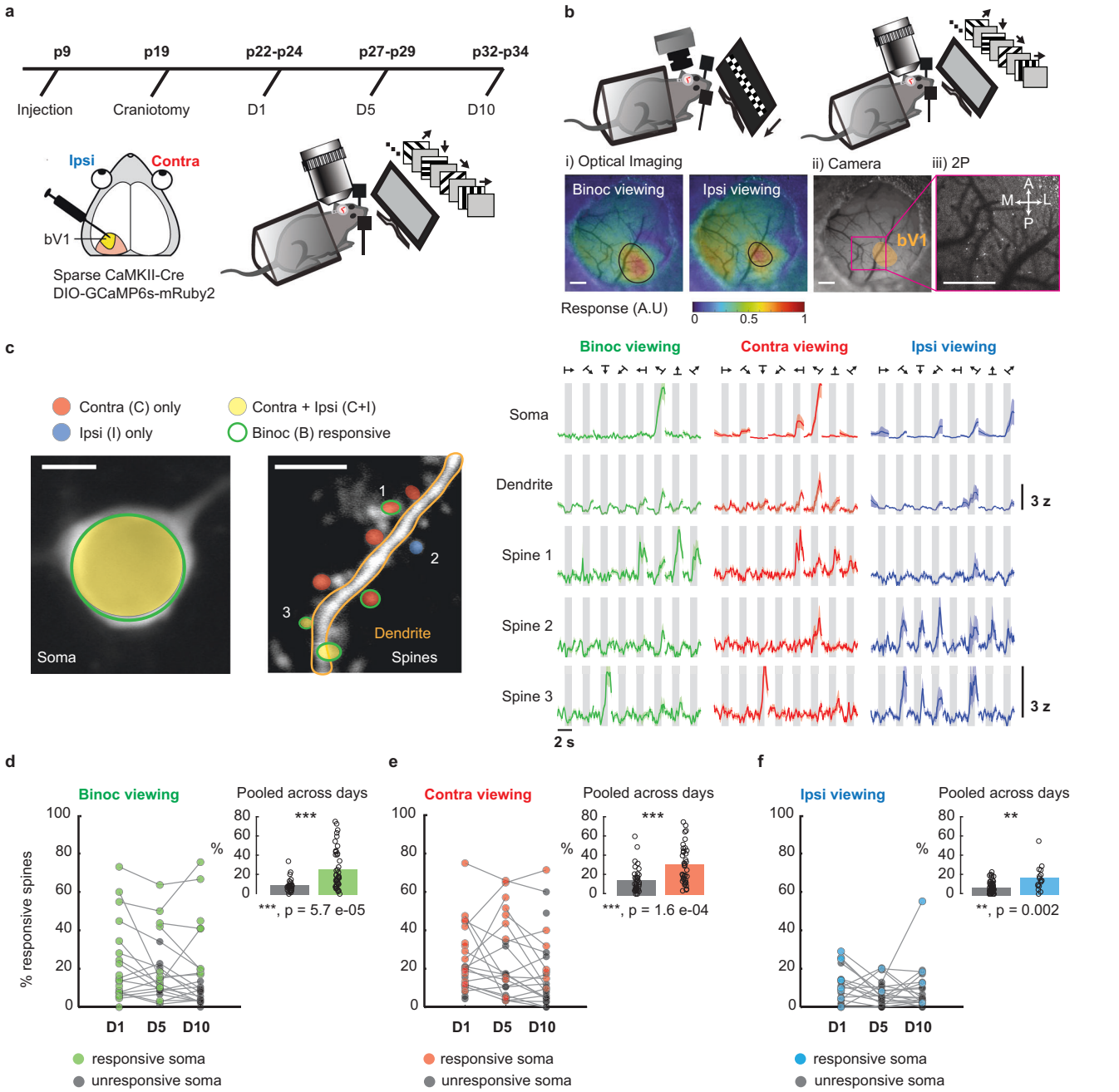

Fig. 1 | Characterizing eye-specific and binocular visual properties of dendritic spines on bV1 neurons during the critical period. a Experimental timeline and recording setup. **b** (**i**) Example response amplitude map recorded during intrinsic optical imaging for binocular viewing (left) and ipsi eye viewing (right). A.U = arbitrary units. (**ii**) Overlay of blood vasculature and area designated as the binocular region of V1. (**iii**) Binocular region imaged on two-photon microscope. Scale bars = 500 μm. **c** (left) Average intensity projection of a soma and dendritic segment recorded on D1 from the same bV1 neuron. Soma and spines are color coded by their responses to the visual stimulus during binoc, contra eye, and ipsi eye viewing conditions. Scale bar = 5 μm. (right) Trial-averaged calcium traces of the soma, dendrite, and three spines responding to each viewing condition. Bolded lines denote the mean and shaded area denotes the standard error across the 10 trials. **d** Proportion of spines recorded from each neuron that were visually responsive to the binoc viewing. Neurons are color coded by whether they were responsive or unresponsive to binoc viewing. $N = 1574$ spines from 26 neurons (D1), 1166 spines from 23 neurons (D5), and 1384 spines from 24 neurons (D10). (inset) Proportion of spines that were visually responsive in neurons that were either responsive or unresponsive to binoc viewing pooled across days. $N = 73$ binocular somatic imaging sessions across neurons and days. **e** Same as (**d**) but for contra eye viewing. **f** Same as (**d**) but for ipsi eye viewing. For (**d**–**f**) inset: two-tailed Wilcoxon rank sum test. Source data are provided as a Source Data file.

condition to determine if these fractions changed over the course of the critical period (Fig. 2g). While the proportion of contra or ipsi responsive spines, on contra or ipsi responsive somata respectively, did not change across the 10 days (Fig. 2g), more spines on binocular responsive somata were responsive during binocular viewing on D10 than on D1, suggesting a developmental increase in binocular drive onto binocular somata.

Rate and timing of calcium events are associated with spine retention

Given the significant turnover we observed in both visually responsive and unresponsive spines over the critical period, we wondered whether spine activity could better predict spine retention, based on prior studies indicating that postsynaptic calcium influx through NMDA

https://doi.org/10.1038/s41467-025-60825-y

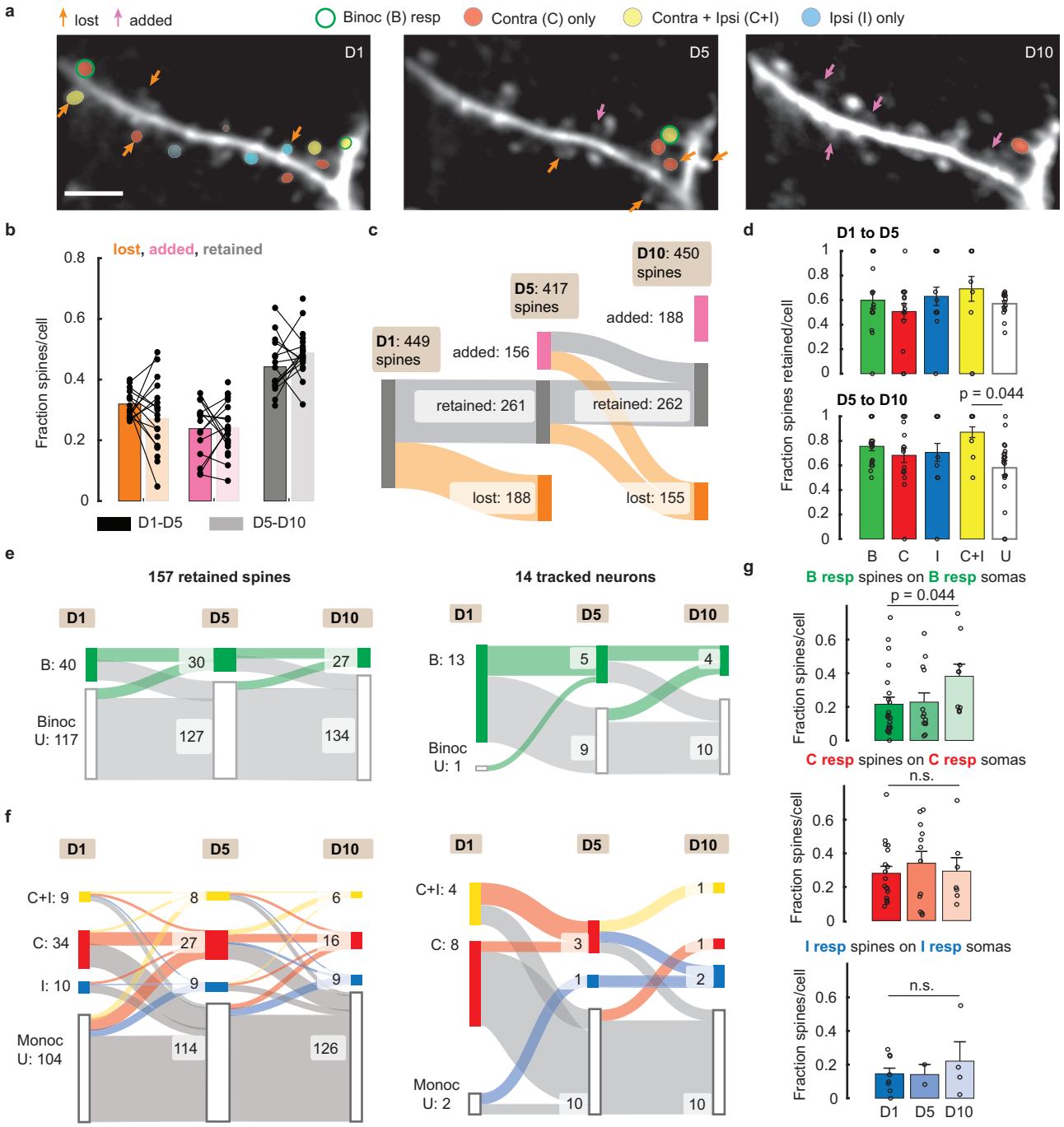

Fig. 2 | Structural and functional dynamics of dendritic spines during the critical period. a Average intensity projection of GCaMP6s fluorescence from a dendritic segment imaged every 5 days during the critical period (D1, D5, D10). Lost dendritic spines are labeled with an orange arrow, and added dendritic spines are labeled with a pink arrow. Scale bar = 5 μm. **b** Fraction of spines per neuron that were lost, added, or retained from D1 to D5 (dark bars) and from D5 to D10 (light bars). $N = 16$ neurons (928 total spines) tracked from D1 to D5, and 20 neurons (1144 total spines) from D5 to D10. Lines connecting points indicate neurons imaged across 3 timepoints (14 neurons). **c** Fate of spines (retained, added, or lost) from D1 to D10. $N = 793$ spines from 14 neurons. **d** Fraction of spines by cell that were retained from D1 to D5 (top) and from D5 to D10 (bottom) based on their response type on D1 or D5, respectively. Points represent the proportion for individual somata (Kruskal-Wallis test and post hoc Dunn's test for response type). $N = 16$ neurons (D1 to D5) and 20 neurons (D5 to D10). **e** (left) Fates of 157 retained dendritic spines chronically imaged from D1 to D10, based on their responsiveness during binoc viewing. (right). Somatic responsiveness of the 14 neurons imaged from D1 to D10. **f** Same as (**e**) but for responsiveness during contra (c) or ipsi (I) eye viewing. Spines and neurons unresponsive to the contra and ipsi eye viewing are denoted as U. **g** Proportion of spines responsive in the same viewing condition (binocular (top), contra (middle), ipsi (bottom)) and timepoint (D1, D5, D10) as their soma. Points represent the proportion for individual somata (Kruskal-Wallis test). Binoc responsive neurons: $N = 22$ (D1), 13 (D5), and 9 (D10). Contra responsive neurons: $N = 19$ (D1), 12 (D5), and 7 (D10). Ipsi responsive neurons: $N = 10$ (D1), 2 (D5), and 4 (D10). For (**d**, **g**): error bars denote the mean ± SEM. n.s. = not significant. Source data are provided as a Source Data file.

https://doi.org/10.1038/s41467-025-60825-y

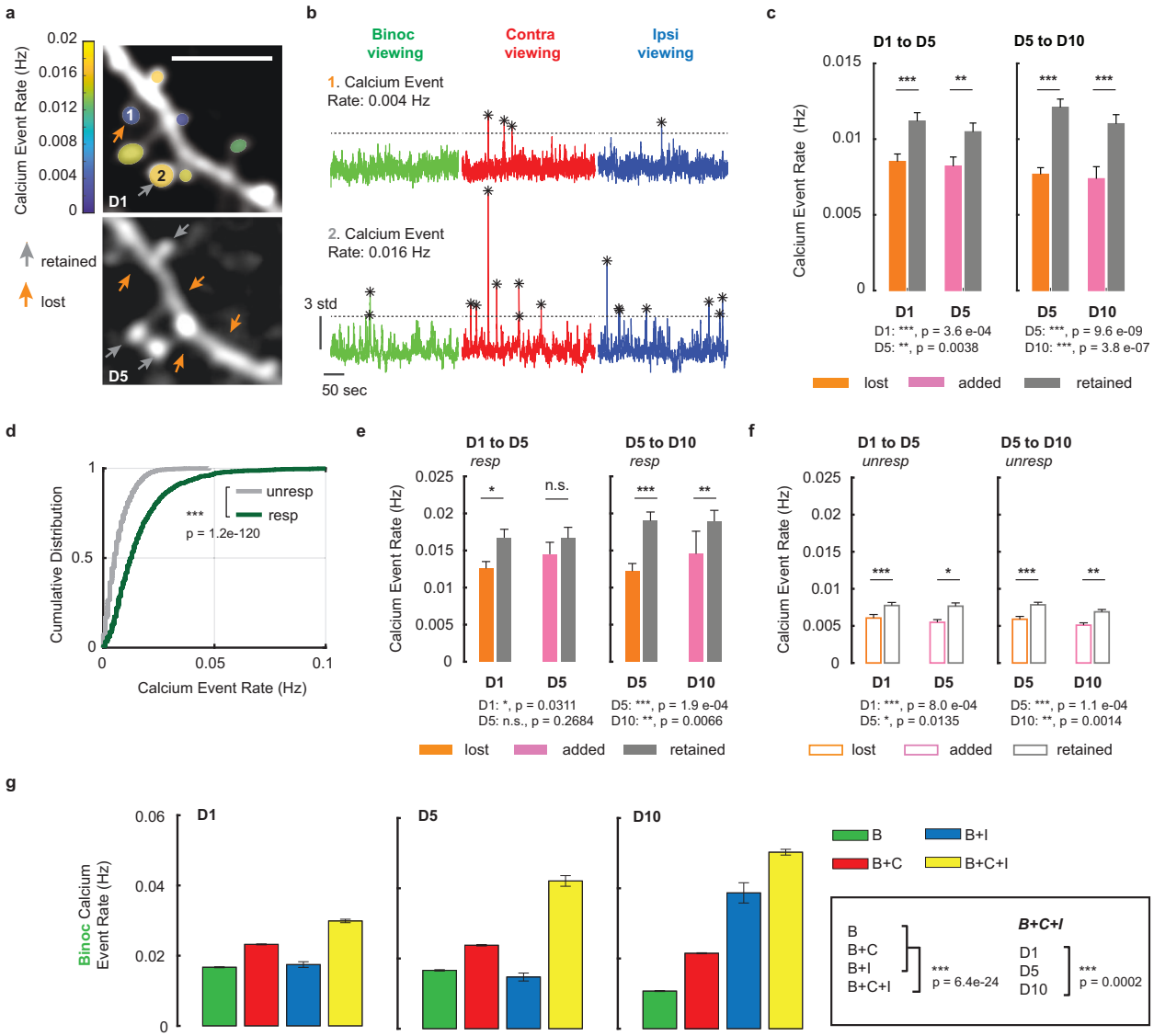

Fig. 3 | Calcium activity is correlated with dendritic spine turnover. a Average intensity projection of a dendritic segment and spines, color coded by calcium activity. Scale bar = 5 μm. **b** Smoothed calcium trace of two dendritic spines from (**a**). Calcium peaks (*) identified using 3 standard deviation threshold. **c** Calcium activity for spines that were lost, added, or retained from D1 to D5 (left) and D5 to D10 (right). D1 to D5: $N = 255$ lost spines, 354 retained spines, and 220 added spines, D5 to D10: $N = 258$ lost spines, 475 retained spines, and 250 added spines. **d** Cumulative distribution of calcium activity in unresponsive and responsive spines. $N = 2848$ unresponsive spines, 1276 responsive spines. **e** Same as (**c**) but for responsive spines (responsive for ≥ 1 condition). D1 to D5: $N = 92$ lost spines (D1), 131 retained spines (D1), 64 added spines (D5), 105 retained spines (D5). D5 to D10: $N = 70$ lost spines (D5), 175 retained spines (D5), 58 added spines (D10), 157 retained spines (D10). **f** Same as (**c**) but for spines unresponsive across all 3 conditions. D1 to D5: $N = 163$ lost spines (D1), 223 retained spines (D1), 156 added spines (D5), 249 retained spines (D5). D5 to D10: $N = 188$ lost spines (D5), 300 retained spines (D5), 192 added spines (D10), 318 retained spines (D10). **g** Binoc calcium activity for spines only responsive to binoc viewing (B), spines responsive to binoc and contra viewing (B + C), spines responsive to binoc and ipsi viewing (B + I), and spines responsive to all 3 (B + C + I). D1: $N = 87$ B spines, 135 B + C spines, 14 B + I spines, 41 B + C + I spines. D5: 66 B spines, 105 B + C spines, 10 B + I spines, 26 B + C + I spines. D10: $N = 77$ B spines, 15 B + I spines, 15 B + I spines, 101 B + C spines, 44 B + C + I spines (two-way ANOVA and post hoc Tukey's HSD for response type and day). For (**c**), and (**e**–**g**): error bars denote mean ± SEM. For (**c**–**f**): two-tailed Wilcoxon rank sum test. n.s. = not significant. Source data are provided as a Source Data file.

receptors can induce long-term potentiation and stabilization in dendritic spines[34–37]. To examine this, we quantified spine activity by measuring the number of calcium events across the binocular, contra eye and ipsi eye viewing conditions at each timepoint (Fig. 3a, b and see Methods for details). While the calcium event rate decreased from D5 to D10 across all spines (Supplementary Fig. 4a, b), retained spines were significantly more active than added or lost spines from D1 to D5 and from D5 to D10 (Fig. 3c). The calcium event rate was correlated with spine retention even when comparing spine activity within a viewing condition (Supplementary Fig. 4c–e), suggesting that elevated calcium activity driven by either eye is sufficient to promote the retention of spines.

To determine whether the rate of calcium activity explained the retention of both responsive and unresponsive spines, we grouped spines into those that were unresponsive across all conditions and those that were responsive to at least one condition. While unresponsive spines were significantly less active than responsive spines (Fig. 3d), dendritic spine activity was significantly higher in both responsive *and* unresponsive spines that were retained from D1 to D5 and D5 to D10 versus those that were lost (Fig. 3e, f). These results thus suggest that calcium activity, even in unresponsive spines, is important for spine stabilization.

We next asked whether spine activity could also explain the significant retention of C + I responsive spines versus other responsive

https://doi.org/10.1038/s41467-025-60825-y

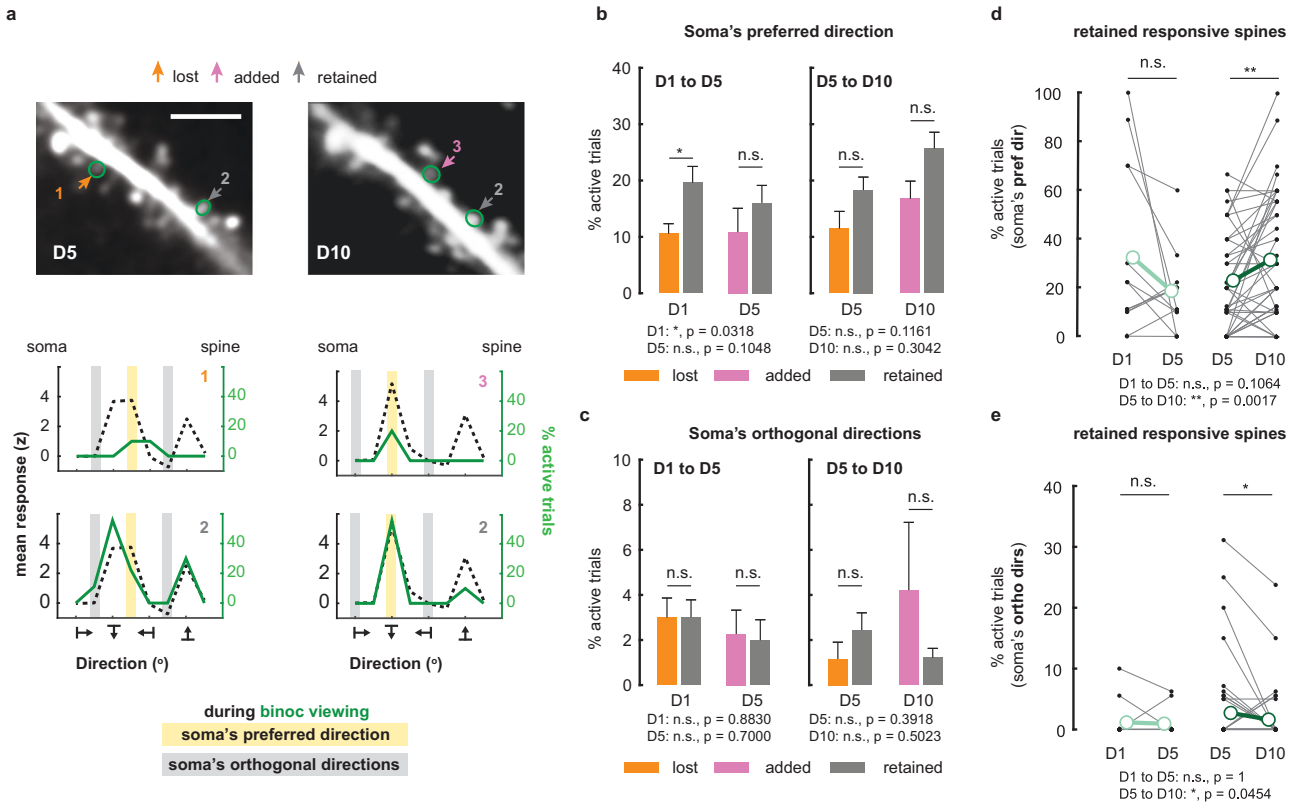

Fig. 4 | Spine retention is linked to its activity at the soma's preferred stimulus. **a** (top) Average intensity projection of a dendritic segment imaged on D5 and D10 with example lost, added, or retained spines labeled. Scale bar = 5 μm. (bottom) Plot of soma's mean response amplitudes for the soma of the above spines across the 8 directions and percent of trials in which the labeled dendritic spine was active during the binoc viewing on D5 (left) and D10 (right). **b** Comparing percent of active trials at soma's preferred direction for visually responsive lost, added, and retained spines from D1 to D5 and D5 to D10. D1 to D5: $N = 62$ lost spines (D1), 70 retained spines (D1), 17 added spines (D5), 28 retained spines (D5). D5 to D10: $N = 24$ lost spines (D5), 65 retained spines (D5), 27 added spines (D10), 85 retained spines (D10) (two-tailed Wilcoxon rank sum test). **c** Same as (**b**) but comparing percent of active trials at directions orthogonal to the soma's preferred direction. **d** Percent of trials in which retained spines were active at soma's preferred direction. D1 to D5: $N = 13$ visually responsive retained spines, D5 to D10: $N = 43$ visually responsive retained spines (two-tailed Wilcoxon signed rank sum test). **e** Same as (**d**) but for directions orthogonal to the soma's preferred direction. For (**b**–**e**): error bars denote the mean ± SEM. n.s. not significant. Source data are provided as a Source Data file.

types over development (Fig. 2d). Here, we focused on the activity during the binocular viewing condition only, as C + I responsive spines would be expected to have higher activity when averaged across all conditions than spines responsive to only contra (C) or only ipsi (I) eye viewing. Therefore, we compared the binocular viewing condition calcium event rate of all monocular response types (unresponsive, C, I, C + I) that were also responsive during binocular viewing (B, B + C, B + I, B + C + I). We found that the binocular event rate of B + C + I responsive spines was indeed higher than for other binocular responsive spines and significantly increased from D1 to D10 (Fig. 3g). For monocular viewing conditions, we also found that C + I spines were significantly more active during the contra eye viewing than C spines on D5 and D10 (Supplementary Fig. 4f), whereas there was no significant difference in the activity rate of I spines vs C + I spines during ipsi eye viewing (Supplementary Fig. 4g). Our results thus suggest that the retention of C + I spines is related to their higher calcium rates. As binocular vision is the condition in which mice normally view the world, and thus the putative driver of experience-dependent synaptic turnover, we focused on the binocular viewing condition in our subsequent analysis.

Previous in vitro and modeling studies have suggested that paired pre- and postsynaptic activity regulates spine strengthening[31,38–40]. To determine whether paired spine and soma activity was linked to the retention of visually responsive spines during the critical period, we compared the fraction of trials in which the spine was active (i.e., had ≥1 calcium event) at the soma's preferred direction during binocular viewing in lost, added, and retained spines (Fig. 4a). Spine activity at the soma's preferred direction was significantly higher in retained dendritic spines than in lost spines from D1 to D5 (Fig. 4b). Surprisingly, this was true even in unresponsive spines (Supplementary Fig. 5a), suggesting that stochastic spine activity coinciding with the soma's preferred stimulus, even if unreliably driven, could still facilitate retention. In contrast, activity at the directions orthogonal to the soma's preferred direction (+/− 90°) was not significantly different between lost and retained spines, for both responsive and unresponsive spines (Fig. 4c and Supplementary Fig. 5b). We further found that retained dendritic spines became more active at the soma's preferred direction (Fig. 4d), and less active at the soma's orthogonal directions (Fig. 4e) from D5 to D10. Our results demonstrate that there is an increase in the specificity of visual input received by retained spines, and thus a change in the tuning of their presynaptic partners, over development.

Average soma-spine alignment increases over development

Based on our findings that the activity of visually responsive spines at the soma's preferred direction was correlated with their retention, we next asked whether the tuning properties of visual inputs during binocular viewing could also contribute to spine retention (Fig. 5a and Supplementary Fig. 6). We did not find a significant difference in the binocular orientation selectivity index (OSI) among lost, added, and retained spines from D1 to D5 (Fig. 5b), though retained spines were

https://doi.org/10.1038/s41467-025-60825-y

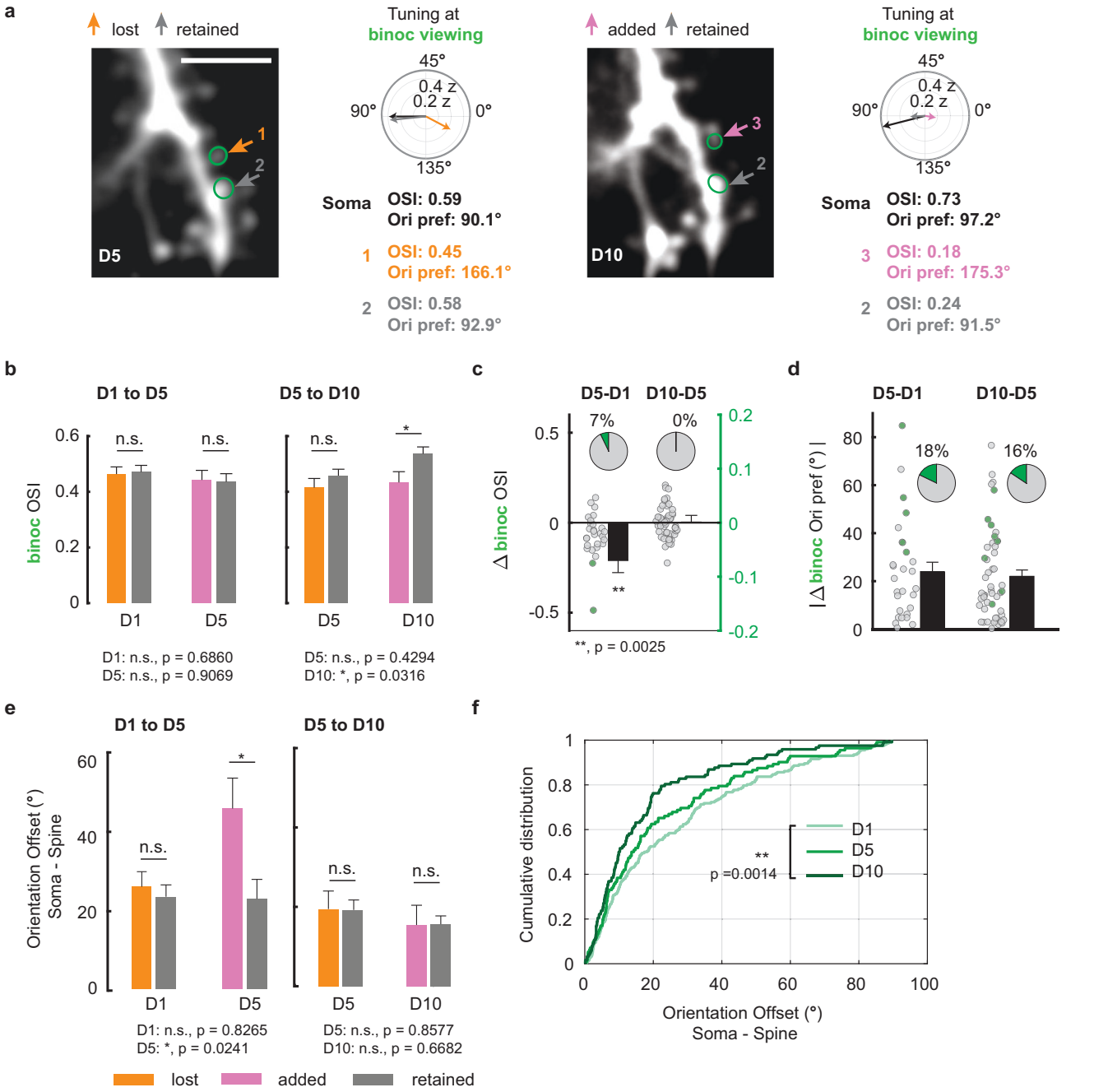

Fig. 5 | Soma-spine alignment increases over development. a Average intensity projection of a dendritic segment imaged on D5 and D10 with example lost, added, and retained spines labeled with arrows. Polar plot of soma and spine's orientation selectivity index (OSI) and preferred orientation (ori pref). Scale bar = 5 μm. **b** OSI in responsive spines during binocular viewing among retained, lost, and added spines from D1 to D5 and D5 to D10. D1 to D5: $N = 63$ lost spines (D1), 78 retained spines (D1), 32 added spines (D5), 51 retained spines (D5). D5 to D10: $N = 39$ lost spines (D5), 101 retained spines (D5), 36 added spines (D10), 107 retained spines (D10) (two-tailed Wilcoxon rank sum test). **c** ΔOSI for retained spines that were responsive during binoc viewing on both D1 and D5 or D5 and D10: $N = 28$ spines (D1 to D5) and 51 spines (D5 to D10) (two-tailed Wilcoxon signed rank test). Pie chart insets denote the portion of retained spines that exhibited significant changes in their tuning compared to a bootstrapped shuffle (labeled as green in scatter). Bar plots (black bar) indicate the mean ± SEM for all retained spines plotted against the green y-axis. **d** Same as (**c**) but for | Δ orientation preference | . **e** Orientation offset from soma for tuned (OSI > 0.3) lost, added, and retained spines from D1 to D5 and D5 to D10. D1 to D5: $N = 46$ lost spines (D1), 58 retained spines (D1), 14 added spines (D5), 22 retained spines (D5). D5 to D10: $N = 20$ lost spines (D5), 53 retained spines (D5), 17 added spines (D10), 67 retained spines (D10) (two-tailed Wilcoxon rank sum test). **f** Cumulative distribution of orientation offset from soma for spines on D1, D5, and D10. $N = 202$ spines (D1), 112 spines (D5), and 122 spines (D10) (Kruskal-Wallis test and post hoc Dunn's test for timepoint). For (**b**–**e**): error bars denote the mean ± SEM. n.s. not significant. Source data are provided as a Source Data file.

more selective to orientations than spines added on D10. Spines that were retained from D1 to D5 experienced a net decrease in their OSI which stabilized from D5 to D10, but only a small fraction experienced significant changes in their selectivity across development (Fig. 5c). The preferred orientation of retained spines shifted on average by 24.1° ± 3.9° (mean ± SEM) from D1 to D5 and by 21.8° ± 2.7° (mean ± SEM) from D5 to D10, with ~16–18% of retained spines experiencing significant shifts in their preferred orientation (Fig. 5d). Together, our results indicate that in bV1, spine retention is not correlated with their selectivity to orientation.

Previous studies have shown that synaptic connectivity between co-tuned neurons increases during postnatal development in mice[5], and we observed increased activity to the soma's preferred stimulus in retained spines. We thus hypothesized that retained or newly added spines would more closely align to the soma's tuning than lost spines, leading to a higher average correlation between soma and spine tuning over development. To test this hypothesis, we compared the soma's preferred orientation to that of tuned (OSI > 0.3) lost, added, or retained spines. We did not find a significant difference in the alignment to the soma's preferred orientation between lost and retained spines from D1 to D5 and D5 to D10 (Fig. 5e). Spines added on D5 were in fact significantly less aligned to the soma's preferred orientation than retained spines. By D10, however, newly added spines were more aligned to the soma and exhibited a similar offset to retained spines, suggesting that the addition of spines is less random later in development, coinciding with the stabilization of somatic visual responses[28,29]. Along with the addition of better matched inputs, there is an overall increase in the spine population's alignment to the soma's preferred orientation from D1 to D10 (Fig. 5f). Our data demonstrate that while the tuning properties of spines do not increase the likelihood of spine retention, better matched newly added inputs may contribute to the net increase in functional alignment between the soma and its inputs.

Correlation among spine pairs becomes more localized over development

While it has recently been shown that neighboring spines on mouse L2/3 excitatory neurons in V1 develop correlated spontaneous activity before the ocular dominance critical period[41,42], it remains unknown whether functional clustering of *visual responses* exists at the start of the critical period or whether this clustering emerges during the critical period. Furthermore, it remains unclear whether correlation to neighboring spines is associated with spine retention during development, as it is during learning[43]. To address these questions, we measured the distance between visually responsive spine pairs and calculated the correlation of their trial-to-trial visual activity during binocular viewing (Fig. 6a).

We first asked whether visually responsive inputs are more likely than chance to synapse next to each other on a dendritic branch and exhibit spatial clustering. On D1, the median distance between visually responsive spines (6.10 μm) was not significantly different than the shuffled median distances across all spine pairs (Fig. 6b and see Supplementary Fig. 8a for only neurons imaged from D1 to D10). By D10, while the median distance between visually responsive spine pairs was unchanged (6.56 μm, Supplementary Fig. 7a), it was now significantly smaller than the shuffled median distances across all spine pairs (Fig. 6b). This suggest that there is an increase in the median distance between unresponsive-responsive, or unresponsive-unresponsive spine pairs. Indeed, we found that the distance between unresponsive-unresponsive spine pairs increased from D1 to D10 (Supplementary Fig. 7a).

To determine whether functional clustering emerges over development, we evaluated the trial-to-trial correlated activity between visually responsive spines as a function of their pairwise distance along the dendrite. Dendritic spines within 5 μm of one another were significantly more correlated than by chance at both D1 and D10 (Fig. 6c, and see Supplementary Fig. 7b for signal, or tuning curve, correlation and Supplementary Fig. 8b for only neurons imaged from D1 to D10). From D1 to D10, the trial-to-trial correlations also significantly increased among neighboring spines within 5 μm, suggesting that there was a developmental increase in spatially proximal, co-active inputs along dendritic branches. Furthermore, by D10, spine pairs at 10 and 15 μm were significantly less correlated than by chance, indicating that distance-dependent potentiation and depression may be engaged to promote functional clustering[44].

To see how the structural turnover of spines contributed to this local organization, we compared the distance and trial-to-trial correlation to nearest neighbors among lost, added, and retained spines. Surprisingly, we did not find a significant difference in the correlation or distance to a nearest neighbor between lost or retained spines from D1 to D5 and D5 to D10 (Supplementary Fig. 7c, d). Likewise, the correlation to a nearest neighbor between added and retained spines was not significantly different over development, though spines added on D10 were significantly closer to neighboring spines than were retained spines (Supplementary Fig. 7c), indicating that the addition of spines could enhance spine clustering observed on D10. In addition, we found that retained spines became more correlated to neighboring spines from D1 to D5 (Fig. 6d), but not between D5 and D10, suggesting that the clustering of retained, co-active spine pairs has largely stabilized after D5.

In modeling studies, functional clusters contribute to somatic drive presumably through the non-linear integration of co-active inputs[45–49], with the influence of such integration largely determined by the size and number of co-active clusters on a neuron[46]. To examine whether these two factors change over development, we defined clusters by identifying visually responsive spine pairs with ≤ 5 μm inter-spine distance and trial-to-trial correlation above their mean pairwise correlation to other responsive spines on the dendritic shaft. On average, the size and number of clusters remained similar from D1 to D10 (Fig. 6e, and Supplementary Fig. 8c for only neurons imaged from D1 to D10), suggesting that these aspects of co-active spine clustering are not significantly altered over development.

Taken together, our results demonstrate that L2/3 neurons exhibit an increase in the correlation among neighboring spine pairs over development, whereas the size and number of clusters remain relatively stable from D1 toD10.

Different forms of synaptic plasticity contribute to spine retention and clustering in a single neuron model

Our observations of spine turnover during the critical period revealed a strong relationship between activity at the soma's preferred stimulus and spine retention, as well as an increase in the correlation among neighboring spine pairs. However, the mechanisms linking these functional properties to structural dynamics of spines and to the refinement of somatic responses remain unclear. We hypothesized that both Hebbian and heterosynaptic plasticity were involved in the retention and clustering of spines, respectively, as these mechanisms have previously been proposed to drive activity-dependent changes in synapses on V1 neurons[25,32,44,50].

To evaluate their putative roles in spine turnover and organization during the critical period, we built a model of a single neuron with two dendritic branches on which orientation/direction selective, eye-specific synaptic inputs experienced Hebbian and heterosynaptic plasticity during a "plasticity period"[51] (Fig. 7). Synaptic density was preserved so that synapses which depressed below a threshold were replaced by new synapses, effectively simulating synaptic turnover. Before the plasticity period, we distributed the visually tuned inputs based on our empirically measured eye-specific proportions on D1 and assigned each input a randomly chosen orientation/direction preference. During the plasticity period, the synaptic strength of each spine changed based on the spine's correlation to the soma and on a distance-dependent correlation to neighboring spines during binocular vision, to incorporate substrates of Hebbian and heterosynaptic mechanisms, respectively[31–33,52,53]. Since an important outcome of bV1 development is the alignment of orientation-specific responses from the two eyes[25,28,29,54], we also measured the soma's orientation preference to binocular, contra eye, and ipsi eye viewing before, during, and after the plasticity period to evaluate the mismatch in somatic orientation preference across the three viewing conditions during this period.

We first asked whether such a model recapitulates our experimental findings on spine retention. By pooling across our simulations (with different initial conditions), we found that a spine's normalized

https://doi.org/10.1038/s41467-025-60825-y

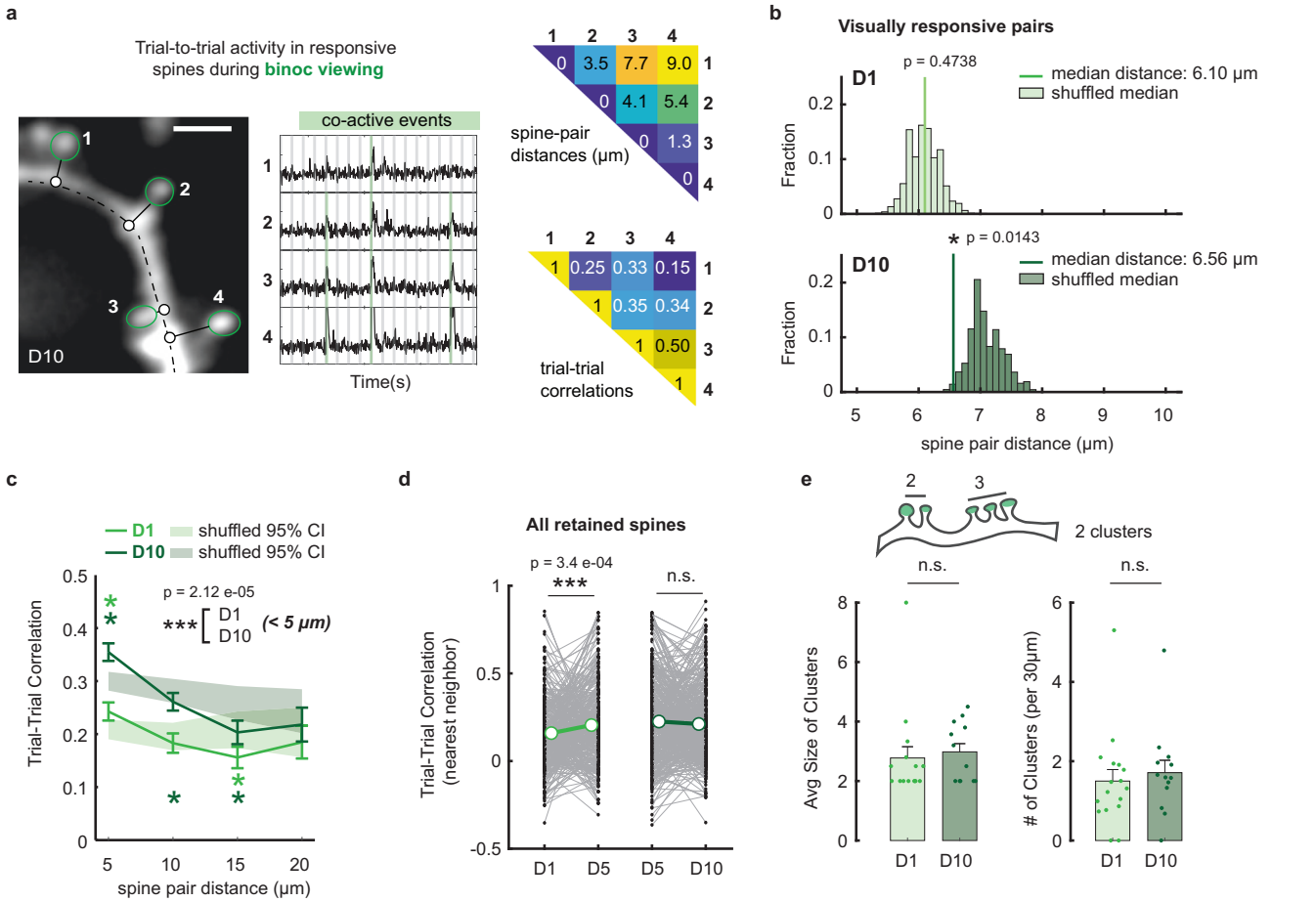

Fig. 6 | Functional clustering of spines increases during the critical period. **a** (left) Average intensity projection of a dendritic segment with the activity traces of the four labeled dendritic spines during binoc viewing shown on the right. Stimulus periods are denoted with gray patches, and co-active events are highlighted in green. Scale bar = 2.5 μm. (right) Pairwise distances and trial-to-trial signal correlations shown for the four spines. **b.** Distribution of median distances among all spine pairs shuffled 10,000 times on D1 and D10. The median distance between visually responsive spine pairs is denoted as a vertical line. $N = 472$ visually responsive spine pairs (D1), and 672 visually responsive spine pairs (D10). p value was found by comparing the true median distance to the shuffled distribution for D1 and D10. **c** Trial-to-trial correlations of visually responsive spine pairs binned by their pairwise distance for D1 and D10. $N = 472$ visually responsive pairs on D1 and 672 visually responsive pairs on D10. Light and dark green asterisks (*) denote distances in which the spine pair correlations fall above or below the 95% confidence interval for the shuffled distribution on D1 or D10, respectively. Correlation between neighboring spine pairs (< 5 μm) increases from D1 to D10 (two-way ANOVA and post hoc Tukey's HSD for spine pair distance and timepoint). **d** Trial-to-trial correlation to nearest neighbor for all spines that were retained from D1 to D5 or D5 to D10. N = 364 retained spines (D1 to D5), and 480 retained spines (D5 to D10) (two-tailed Wilcoxon signed rank test). **e** (left) Average number of co-active responsive spines within a cluster per cell from D1 to D10. (right) Average number of clusters per cell normalized to a 30 μm dendritic length from D1 to D10. Error bars denote mean ± SEM. $N = 17$ neurons (D1), $N = 13$ neurons (D10) (two-tailed Wilcoxon rank sum test). n.s. not significant. Source data are provided as a Source Data file.

activity (quantified from the presynaptic accumulator, see Methods) was significantly correlated with its survival time during the plasticity period (Fig. 8a). Spines retained at the end of the plasticity period were more active and more correlated to the soma than lost spines, which aligns with our experimental finding that retained spines had a higher rate of calcium events (Fig. 8b), especially in response to the soma's preferred stimulus (Fig. 8c), than spines lost over the 10-day critical period. Furthermore, the correlation between neighboring spines increased significantly after the plasticity period, and the difference between post- and pre-plasticity period correlation values binned by distance followed a similar pattern to that observed in vivo between D10 and D1 (Fig. 8d). Our simulations thus indicate that a combination of Hebbian and heterosynaptic mechanisms plausibly underlie the retention and clustering of dendritic spines we observe during development.

Beyond capturing experimental observations, we next tested the individual contributions of these mechanisms to somatic orientation matching. For the Hebbian component, we varied the influence of somatic back-propagating events, and for the heterosynaptic component, the neighboring spine activity on a spine's strength during the plasticity period (Supplementary Fig. 9). We found that heterosynaptic plasticity was necessary for increasing the correlation between neighboring spines (Supplementary Fig. 9a). On the other hand, incorporating Hebbian or heterosynaptic plasticity was sufficient for decreasing the mismatch between ipsi and binocular viewing responses (Supplementary Fig. 9b). Taken together, our simulations indicate that Hebbian plasticity alone is not sufficient to explain our in vivo observations, and thus heterosynaptic plasticity likely contributes to spine retention, organization, and somatic orientation matching during the critical period.

Discussion

Structural and functional changes in synapses drive critical period development

L2/3 neurons in mouse bV1 experience significant changes in their visual responses during the critical period[25,28,29]. Yet, little is known

https://doi.org/10.1038/s41467-025-60825-y

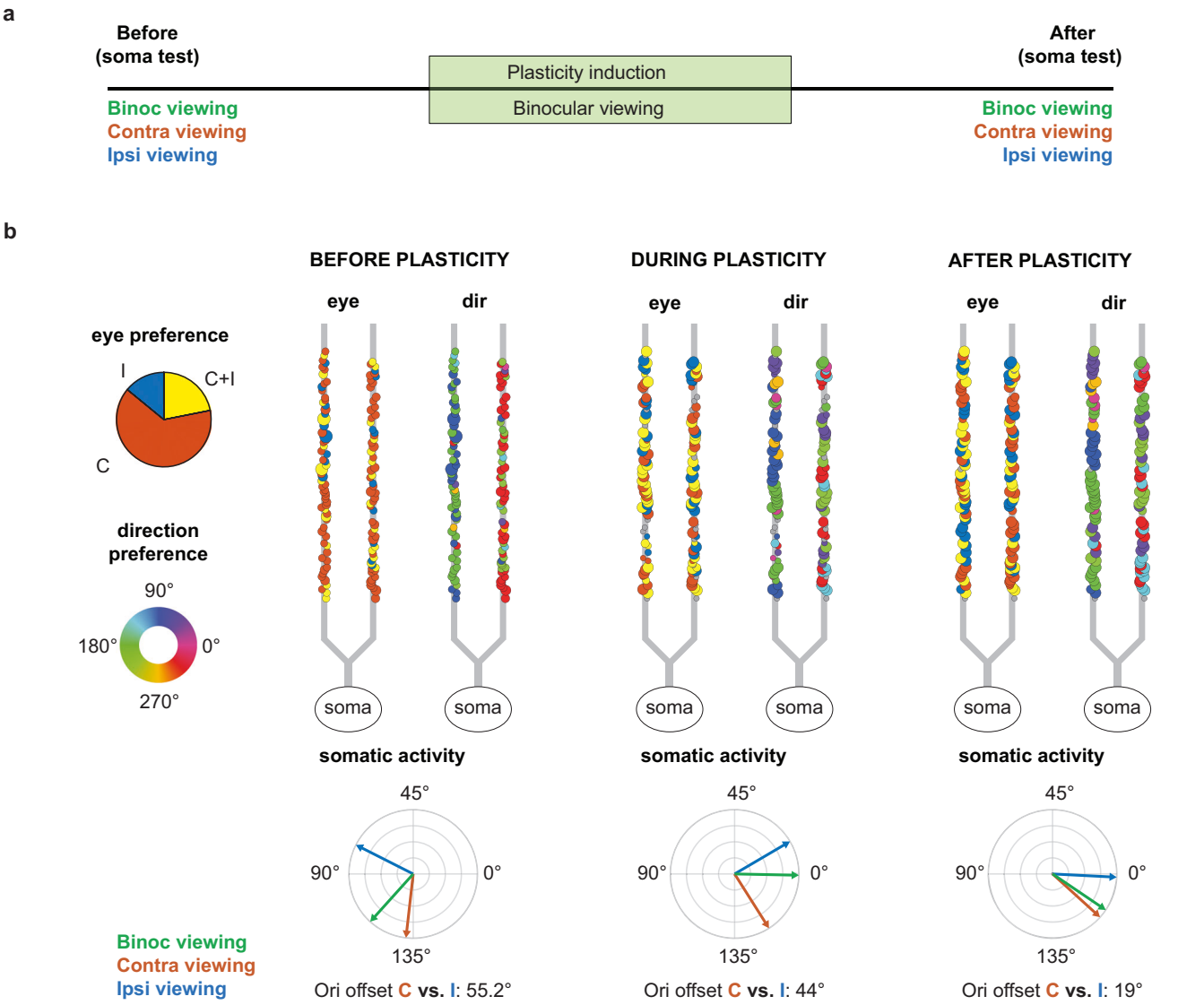

Fig. 7 | Simulating Hebbian and heterosynaptic interactions in a single neuron model. a. Schematic of the model. Before and after plasticity, somatic responses to 8 directions are measured for the three viewing conditions (binoc, contra, and ipsi eye). During the plasticity period, synaptic inputs are driven only to binoc viewing and the synaptic strength of each spine changes based on Hebbian and heterosynaptic plasticity rules defined in the model. **b** Example trial simulating functional and structural dynamics of spines before, during, and after the plasticity induction period. (top) Before plasticity, visual inputs are distributed based on the empirical eye-specific proportions found at D1 and randomly assigned a preferred direction (pie chart and color wheel on left). The soma with its two branches is shown for three timepoints (before, during and after plasticity, from left to right). For each timepoint, the colors in the left and right schematic represent the eye and the direction (dir) preferences of the spines, respectively. (bottom) Polar plot depicting the binoc, ipsi, and contra orientation preference of the soma (denoted by the arrow) at the three timepoints.

about the synaptic mechanisms that underlie these developmental shifts, as no previous study has tracked the synaptic responses of bV1 neurons across the critical period. By performing longitudinal two-photon calcium imaging of sparsely labeled L2/3 neurons from ~p22 to p32, we show that turnover of synapses is significantly correlated with their visually driven activity and the degree to which they are active at their soma's preferred stimulus. The retention we observe of dendritic spines – at about 40% across the 10 days (Fig. 2), is about two times lower than what has been reported in adult or even in post-critical period mice (~80–90%)[30,55,56], suggesting that this heightened turnover is a defining feature of the critical period and underlies the reconstruction of binocular inputs to V1 neurons[28]. It is possible that spines classified as retained were eliminated and replaced by a newly added spine formed in close proximity to the eliminated spine, and were thus misclassified as retained (see Supplementary Fig. 10). While shorter intervals may suggest lower retention due to increased sensitivity to turnover, this would only reinforce our conclusion that significant turnover occurs during the critical period.

We also find that ~50% of newly added spines are lost after 5 days, demonstrating that new spines are less likely to be retained than existing spines. The transient nature of excitatory synapses has been described across different species[57], brain areas[58], and developmental timepoints[30,55,59], indicating that sampling and consequent re-structuring of presynaptic inputs is prevalent in neural circuit refinement. Despite this high degree of turnover, the density of spines remains stable (Supplementary Fig. 3), suggesting that changes in visual responses at the somata are not due to shifts in excitatory synapse number. On the other hand, the eye-specific responses of dendritic spines are highly dynamic, consistent with the instability measured in the bV1 L2/3 neuronal population during the critical

https://doi.org/10.1038/s41467-025-60825-y

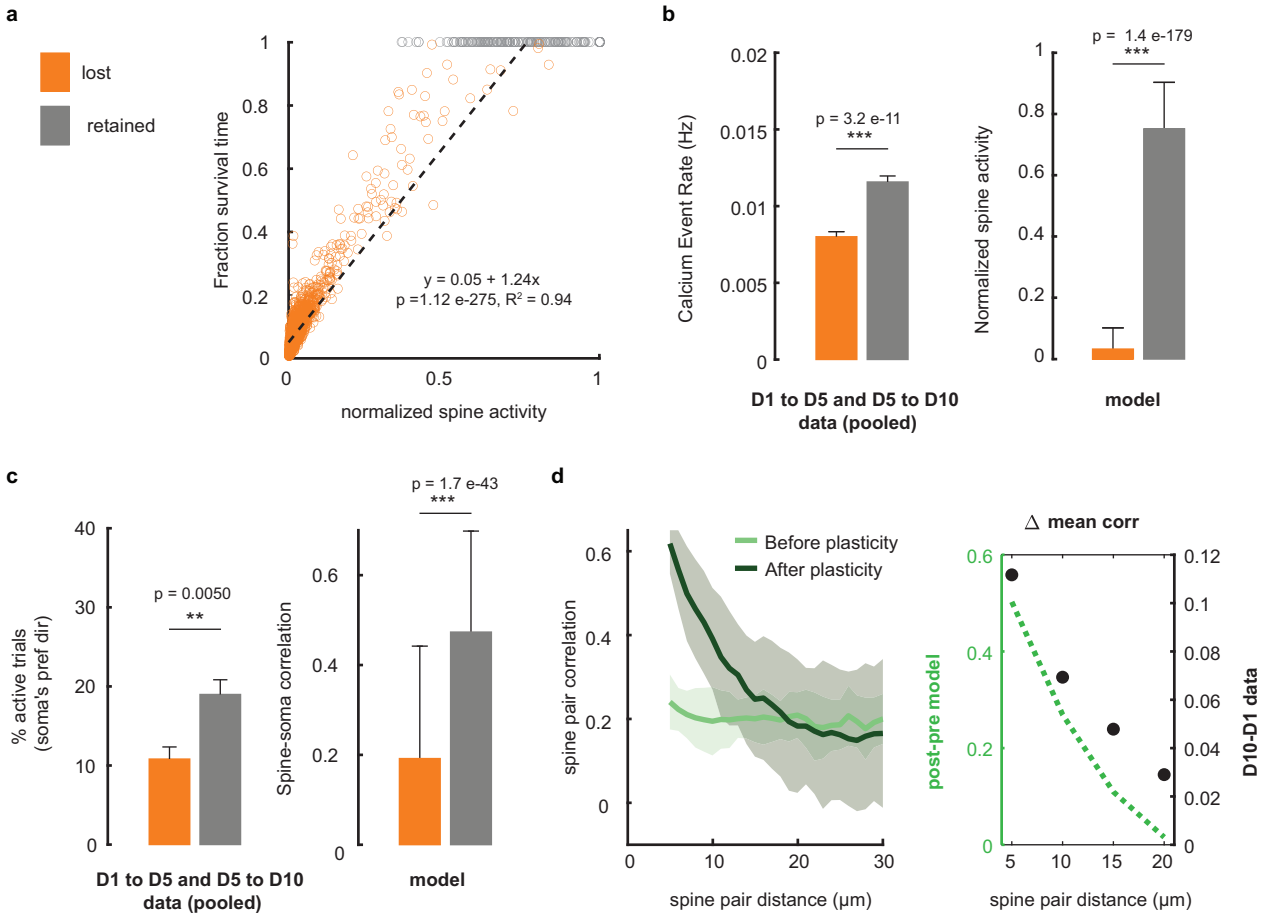

Fig. 8 | Hebbian and heterosynaptic interactions contribute to retention and clustering of spines in a single neuron model. a Linear regression between the spine's fraction survival time and normalized activity. $N = 2560$ spines from 20 simulations. **b** (left) Comparing calcium event rate between 513 lost and 829 retained spines (using data from Fig. 3 pooled across D1 to D5 and D5 to D10). (right) Comparing normalized activity (based on presynaptic accumulator) between lost spines and retained in the model. $N = 316$ retained spines and 2244 lost spines. Error bars denote the mean ± SEM in data and mean ± standard deviation in model. **c** (left) Comparing percent of trials in which spine was active at the soma's preferred direction between 86 lost and 135 retained spines (using data from Fig. 4 pooled across D1 to D5 and D5 to D10). (right) Comparing correlation to soma between lost and retained spines in the model. Error bars denote the mean ± SEM in data or model. **d** (left) Spine pair correlations as a function of spine pair distance. Shaded areas represent mean ± standard deviation in model. (right) Comparing the delta mean correlation between the before- and after-plasticity period from model (dashed green line) and between D1 and D10 from experimental findings (black dots) binned by spine pair distance. For (**b**–**d**), two-tailed Wilcoxon rank sum test. Source data are provided as a Source Data file.

period[28]. Taken together, our findings suggest that the elevated turnover of excitatory synapses, as well as the shifts in visual properties of retained, presynaptic inputs, contribute to the shaping of somatic responses during development.

Role of synaptic activity in spine retention and clustering

Our findings revealing the strong link between spine activity and retention (Fig. 3) support the fundamental role calcium entry plays in stabilizing and strengthening dendritic spines[60]. This suggests that the activity level of presynaptic inputs is an important regulator of binocular visual circuit development. Indeed, the relative activity between ipsi and contra inputs has been robustly shown to drive competition between eye-specific inputs during monocular deprivation[14,61,62]. Notably, we find that spines responsive to the contra and ipsi eye (C + I spines) are more active than spines responding only to the contra or ipsi eye, and that C + I spines are more likely to be retained over development (Fig. 2). As the emergence of responsiveness to both eyes is a defining feature of bV1 (but see[7,8,28,29]), this suggests that the activity and retention of intracortical presynaptic connections are crucial drivers of bV1 circuits.

Surprisingly, we find that a majority of dendritic spines on L2/3 neurons become unresponsive to visual stimuli over the course of the critical period (~80%) (Fig. 2e,f). Furthermore, out of the unresponsive spines at p22-24 that had been retained until p32-p34, about 80% remained unresponsive (Fig. 2). What factors explain the retention of these unresponsive spines, and what possible function(s) could they serve for the neuron? Interestingly, we found that retained unresponsive spines are more active than lost unresponsive spines (Fig. 3). This elevated activity in unresponsive spines could serve a homeostatic role to maintain baseline excitability and overcome the sparsity of visually driven inputs. Furthermore, 'non-visual' inputs have been shown to contribute to population-level encoding in V1 in a visual discrimination task[63], and thus the retention of unresponsive inputs could be critical for regulating neural computations during visual processing. It is indeed possible that many synapses we deemed unresponsive are, in fact, responsive to, or strongly modulated by, non-visual input, such as motor actions or arousal[64–66], or are unreliably activated by visual stimuli[67], or are responsive to visual stimuli not included in our stimulus set. It is important to also note that a large proportion of the neurons we sampled at D1 do become unresponsive by D10 (Fig. 2, Supplementary Fig. 11), which is associated, but not significantly, to a decrease of visually responsive spines ($p = 0.063$, Supplementary Fig. 11d). The loss of visually-driven responses is unlikely to be related to AAV toxicity or laser damage, as we confirmed the

health of the neurons at each time point (see Methods for details) and did not observe a significant difference in the neurons' baseline activity level between D1 and D10 or between neurons that were responsive and unresponsive to the visual stimuli (Supplementary Fig. 11b). While the proportion of neurons we observe gaining and losing visual responsiveness differs from a prior, chronic population imaging of bV1 neurons during the critical period[28], this is likely due to our intensive spine-based analysis of fewer neurons compared to the soma-based analysis of a larger population of neurons in the previous study.

Despite the "salt and pepper" spatial organization of orientation preference in the mouse visual cortex, studies have shown that functionally correlated neurons in L2/3 exhibit biased connectivity and thus form functional microcircuits[68–71]. This "like-to-like" connectivity increases over postnatal development, and is thought to contribute to the refinement of visual responses[5,72]. Our results show that a higher fraction of dendritic spines become aligned to the soma's preferred orientation by the end of the critical period (Fig. 5) and that retained spines are more active at the soma's preferred stimulus than spines that are lost over development (Fig. 4), indicating that "like-to-like" connectivity could emerge, at least in part, through activity-based retention. The offset of the spine's orientation preference from the soma's, however, was not predictive of spine retention, suggesting that shared tuning is not required for retention. Instead, our results imply that as long as the spine surpasses some activity threshold at the soma's preferred stimulus, it will be retained. These "like-to-like" inputs are unlikely to be thalamocortical inputs, as recent works has shown that only 6% of inputs onto L2/3 excitatory neurons originate from LGN inputs[73]. Furthermore, we observed selective retention of spines responsive to both eyes, whereas input from the LGN is largely monocular[74]. Thus, our findings corroborate previous studies suggesting that the observed increases in "like-to-like" connectivity in developing mouse V1 is a cortical phenomenon reflecting activity dependent plasticity of corticocortical connections.

Our findings also demonstrate that the trial-to-trial activity of neighboring spines are significantly correlated (within 5 μm), corroborating previous studies in adult mice[75–77]. We further show that the correlation among neighboring spine pairs increases over development (Fig. 6), whereas the correlation among more distant spine pairs decreases. It is possible that functional clustering arises through the addition of multiple synapses from a single presynaptic axon; however, a recent EM study in mouse visual cortex found that only 11% of connections between L2/3 neurons are multi-synaptic[78]. It is, therefore, likely that clustering increases due to heterosynaptic interactions between neighboring spines. Though we did not find a difference in the correlation among lost, added, or retained spines to their neighboring spines (Supplementary Fig. 7), we did find that retained spines became more correlated to their neighbors over development. Our results thus suggest that this increase in co-activity could be attributed either to the loss or addition of spines next to a retained spine or to the change in the activity of a neighboring retained spine. To distinguish between these two scenarios, it will be critical to track the structural and functional properties of spines across smaller time intervals.

Modeling the emergence of somatic orientation matching reveals putative mechanisms for synaptic change

While our study has identified that the retention of spines is strongly linked to their activity levels and that clustering of neighboring spines increases over development, the molecular drivers of these synaptic changes remain unclear. For decades, bV1 has served as a model system to study these mechanisms of plasticity due to the lowered plasticity threshold which defines the ocular dominance critical period and the ease with which visual experience can be manipulated[1,9–11]. Two broad classes of plasticity known to be inducible in V1 are Hebbian and heterosynaptic plasticity[32,44], which are driven by the correlation between pre- and post-synaptic responses and between neighboring spines, respectively. While the relevance of these mechanisms in the context of normal bV1 development is unknown, they would seem to fit our experimental findings well; the preferential retention of spines active at the soma's preferred stimulus could putatively be driven by Hebbian potentiation and the increase in correlation between responsive, neighboring spines could putatively be driven by heterosynaptic potentiation or depression[32]. Despite the plausibility of these mechanistic hypotheses, they are challenging to address in vivo due to the difficulty of isolating and distinguishing Hebbian and heterosynaptic effects without perturbing other cellular mechanisms or normal developmental experience.

Therefore, we built a single neuron model based on our experimental observations to examine the effects of altering Hebbian and heterosynaptic plasticity rules on synaptic turnover and somatic refinement. We indeed found that incorporating both mechanisms into a single neuron model validates our in vivo findings. Modeled spine activity is higher in retained spines than in lost spines, and the correlation between nearby spine pairs increases after the simulated plasticity period. Removing heterosynaptic interactions blocked the localized clustering of correlated spine pairs, whereas both Hebbian and heterosynaptic plasticity were sufficient for aligning the somatic orientation preference of ipsi eye inputs over the plasticity period. Based on our simulations, we propose that both mechanisms are necessary during the critical period to drive the turnover of spines that are misaligned to the soma and to neighboring spine pairs, which ultimately lead to refinement of bV1 responses, such as orientation matching between the two eyes.

In our study, we tracked the functionally identified synaptic inputs to spines on individual bV1 neurons during the critical period in mice. Our approach has been crucial for linking the structural turnover of dendritic spines to their visually driven responses, and hence their contribution to somatic visual responses. We have thus revealed fundamental properties of spines that are lost and retained, properties of spines that are added, the activity-dependent local organization of spines, and the putative roles for Hebbian and heterosynaptic plasticity in regulating experience-dependent refinement of neuronal responses. Our study highlights the extraordinary degree of synaptic change that underlies the construction of functional circuits during normal development in a relatively brief period of heightened plasticity driven by sensory experience.

Methods

Experimental model and subjects

All procedures performed in this study were approved by the Massachusetts Institute of Technology's Animal Care and Use Committee and conformed to the Guide for the Care and Use of Laboratory Animals published by the National Institutes of Health. Male and female wild-type C57BL/6j mice were used in study. Mice were group housed post-weaning (no more than five mice per cage) with a standard light/dark cycle of 12/12 hours with access to food and water *ad libitum*. On average, temperature was 70° F (21 °C) and humidity was 50%.

Stereotaxic surgery procedures

Viral injection. Postnatal (p) day 9–10 pups were anesthetized with isoflurane (3% for induction, 1–1.5% for maintenance) and placed on a stereotaxic apparatus (Kopf) while maintaining a body temperature of 37.5 °C using a heating pad (ATC2000, World Precision Instruments). Pre-operative slow-release buprenorphine (1 mg/kg, subcutaneous injection) and meloxicam (5 mg/kg, subcutaneous injection) was provided to mice before surgery. Once the appropriate level of anesthesia was achieved, fur was removed from the surgical site with Nair. Skin was cleaned with saline, betadine, and 70% ethanol three times with a cotton applicator. The scalp was then scored with a scalpel and the skin was folded back to expose the skull. We injected through the skull using stereotaxic coordinates for the left hemisphere of the binocular

region of the visual cortex (0.5–1 mm anterior from the lambda suture and 3 mm lateral from the midline suture). AAV9.CaMKII.Cre (~1e10 vg/ml, Addgene) and AAV1-hSyn1-Flex-mRuby2-GSG-P2A-GCaMP6s-WPRE-SV40 (≥1e13 vg/ml, Addgene) was mixed at a 2 to 3 ratio and 150 nL of the virus was injected at 50 nL/min (0.2–0.25 mm below the dura to target L2/3) using a pulled, glass pipette with a 50 µm diameter, beveled tip. We repeated this procedure 1-2 times at injection sites that were 500 µm apart. All injections were performed using an infuser system (QSI 53311, Stoelting) attached to the stereotaxic frame. Following the injections, the skin was sutured with internal stitches (Prolene 7.0), and the pups were returned to the dam cage to recover.

Craniotomy and Head-plate Implant. 9-10 days after the viral injection, mice were anesthetized and prepared for surgery using the same procedure as in *Viral Injection*. Following the scoring of the scalp and retraction of the skin, we drilled a 3 mm circular hole over the binocular region of the primary visual cortex, centered at 1.5 mm anterior from the lambda suture line and 3 mm lateral from the midline suture, in the left hemisphere using a dental drill. Two 3-mm coverslips centered on a 5-mm coverslip (CS-3R and CS-5R, Warner Instruments) were glued together with optical adhesive (#NOA 61, Norland), and positioned over the craniotomy. The coverslip was then attached to the skull using Metabond mixed with a black ink pigment (Black Iron Oxide 18727, Schmincke). A custom designed stainless-steel head-plate was then positioned over the coverslip and attached to the skull with Metabond (C&B Metabond, Parkell).

Two-photon Imaging

Mice were head-fixed on a custom-built behavior rig and placed in a polypropylene tube to constrain movement. Two-photon imaging was done through the cranial window over the binocular region of the primary visual cortex in mice using resonant-galvo scanning with a Prairie Ultima IV two-photon microscopy system. For all recordings (soma and dendritic segments of neurons), we used a XLPlan N 20 × 1.00 NA or 25 × 1.05NA (Olympus) objective and an excitation wavelength of 920 nm using the Ti:Sapphire tunable laser (Mai-Tai eHP, Spectra-Physics). Somatic imaging was done at a resolution of 5.24-25.00 pixels μm^{-1}, whereas dendritic imaging was done at a resolution of 15.15–25.00 pixels μm^{-1}. We acquired recordings at 512 × 512 resolution with a final frame rate of about 7.75 Hz after 4-frame averaging. To align the recording with the visual stimulus played during two-photon imaging, we used a data acquisition device (BNC-2110, National Instruments) to send an analog voltage signal to the two-photon microscope at the onset of each visual stimulus presentation. Each neuron was imaged for ~2 hours (soma and 3-4 dendritic segments) per timepoint. Neuronal health was assessed at each time point by the lack of GCaMP6s signal in the nucleus, low frequency of spontaneous high amplitude transients, and lack of blebbing of the dendritic processes. We selected somata residing 100-200 µm below the surface, and sampled segments from basal, oblique, and apical dendrites. For each somatic and dendritic recording, we had three separate viewing conditions in random order: binocular viewing, ipsilateral eye viewing, and contralateral eye viewing. Mice were imaged every 4–5 days for a period of 10 days, starting from ~p22-p24 to ~p32-p34, to encompass the critical period for somatic orientation matching[25,28,54].

Visual stimulus for Two-photon Imaging

An LCD monitor (11.6-inch, 60 Hz refresh rate, LONCEVON) was placed 9 cm in front of the mouse to display the visual stimulus. The monitor covered ~100° in azimuth and ~60° in elevation, and had a mean luminance of 35 cd/m^2. During two-photon imaging, we presented awake mice with drifting grating stimuli using the Psychophysics Toolbox in MATLAB. We used high-contrast, drifting sinusoidal gratings at 8 different directions separated by 45° intervals with a temporal frequency of 2 Hz, and a spatial frequency optimized to the soma's preferred frequency during binocular viewing at the first day of recording (sampled at 0.02, 0.04, and 0.08 cycles per degree). 10 trials of each grating were presented in a pseudorandom order with a 3 second gray screen inter-stimulus interval.

Optical Imaging

To determine whether the injection site was within the binocular region of the primary visual cortex, optical imaging was performed on 10/15 mice. Mice were head-fixed on a behavioral rig and lightly anesthetized with isoflurane (0.5%-1%) to minimize movement. A 70 cm x 34 cm monitor was placed at a 45° angle 22 cm from the mouse's head to cover 115° in azimuth and 75° in elevation. Green light (560 nm) was first used to focus on and image the cortical surface for alignment to two-photon imaging. Functional imaging was then performed using red light (630 nm) and a focus 400 µm below the surface. To capture the change in reflectance of the red light, an electron multiplying CCD camera (Cascade 512B; Roper Scientific) was used, imaging at 30 Hz with 4 × 4 on chip binning. Mice viewed a contrast-reversing checkerboard bar that was 30° wide, drifting upward or downward and repeated 20 times at 12 seconds/cycle. To calculate the strength of visually driven responses for each eye, we performed a Fourier Transform of the time-series data for each pixel at the stimulus frequency (12 Hz), and computed the amplitude of the Fourier Transform using custom written python scripts (https://github.com/Palpatineli/oi_analyzer). The binocular zone was defined as the cortical region that was driven by both the ipsilateral and contralateral eye.

Analysis for Two-photon Imaging Data

Preprocessing. To correct for the motion present during two-photon imaging and to align each condition, we concatenated the recordings of GCaMP6s signal for each FOV (soma or dendritic segment) during binocular, ipsilateral eye, and contralateral eye viewing. We then registered each frame to the average intensity projection of the FOV using the Template Matching plugin in ImageJ, and repeated this procedure 2 times. Elliptical ROIs were then manually drawn over the dendritic spines (or soma) and small rectangular ROIs were placed directly under each dendritic spine along the dendritic branch. The average fluorescence intensity within the ROI was calculated for each frame, and the time-series raw fluorescence values were exported to MATLAB for subsequent analysis.

Registration across multiple timepoints. We registered dendritic segments imaged across multiple timepoints using a semi-automated process using the average intensity projections of the dendritic segments. First, we measured the distances between dendritic spine coordinates projected onto the dendritic branch and marked fiducial points (i.e., branch points, stable spines) using custom code written in Python. We then compared the distances for segments imaged between two timepoints (i.e D1 and D5). If the distance for spine X at D1 and spine Y at D5 to a fiducial was the same within ±1 µm, we considered spine X and spine Y to be the same spine, and thus retained. If there were no spines with distances to the fiducial point matching spine X or Y in the compared timepoint[79], then we considered the spine either lost or added, respectively. Of note, the experimenter was blinded to the timepoints of the imaged FOVs when verifying the alignment *post hoc*.

Tuning properties. To normalize the raw fluorescent values, we computed a Z score for each frame: $Z = \frac{F(t) - mean(F_{baseline})}{std(F_{baseline})}$, where $F_{baseline}$ was found by concatenating all the interstimulus periods up to one second before the onset of each stimulus[7,44]. For the dendritic spines, we subtracted signal coming from backpropagating action potentials by performing a robust regression against the dendritic signal as done

previously[75,77,80–82]. We quantified the overall calcium event rate of spines by concatenating the Z scored traces across the three conditions (or using only the binocular viewing condition) and applying an exponentially weighted averaged filter[82]. Calcium peaks that passed the 3 standard deviation threshold for 3 frames were defined as calcium events[80]. For characterizing stimulus aligned calcium activity, we removed trials where the peak baseline activity was above three standard deviations (somas and spines) or where there was motion artifact during the trial based on the mean activity of the dendritic shaft dropping below 2 standard deviations (spines only). To identify visually responsive somata and dendritic spines, we applied three criteria for each unique stimuli: 1) the fraction of trials remaining after exclusion with the above criteria was ≥50% (5/10 trials), 2) the mean amplitude response R(q) was above 0.5 Z (measured to be the 99.8 percentile of 'responses' aligned to the interstimulus periods), where R(q) was found by subtracting the mean pre- from post-stimulus activity trace and taking the average across the 10 trials, and 3) a Student's paired-t test between the mean pre-and post-stimulus activity trace ($p < 0.05$)[7]. To determine the false discovery rate of our response criteria, we randomly selected timestamps from the recording as stimulus onset times and identified spines that passed our criteria with these "scrambled" trials, repeated 10,000 times. On average, the false discovery rate for dendritic spines pooled across viewing conditions and days was 4%.

In visually responsive somata and dendritic spines, we computed their orientation tuning properties using a vector based approach[83]. To determine the direction selectivity, we used the trial-averaged response amplitudes taken across the 8 directions, and calculated the length of vector L_{dir}, where $L_{dir} = \frac{\sum_k \mathrm{R(q}k) \exp(i\mathrm{q}_k)}{\mathrm{R(q)}}$. Similarly, we calculated the orientation selectivity by the length of L_{ori}, where $L_{ori} = \frac{\sum_k \mathrm{R(q)} \exp(2i\mathrm{q}_k)}{\mathrm{R(q)}}$. R(q$k$) is the response at direction k or at the orientation k (taken by averaging the response across the 2 opposing directions). To determine the preferred orientation or direction of the grating, we took the arctangent of the imaginary and real component of vector L, to find the corresponding angle.

Soma-Spine correlation analysis. To determine the alignment of spines to the soma's preferred stimulus, we measured the fraction of trials in which there was a spine calcium event (ie. an active trial) at the direction in which the soma had a maximum response. We also compared the alignment between the spine and soma's tuning by taking the difference between their preferred orientation: $\Delta\theta = |\theta_{spine} - \theta_{soma}|$ or by taking the Pearson's correlation coefficient correlation between the mean amplitude responses across the 8 directions. Only visually responsive tuned spines (OSI > 0.3) were considered for the orientation offset analysis.

Spine clustering analysis. To quantify whether dendritic spines are functionally clustered along a dendritic segment, we measured the pairwise distances between dendritic spines' coordinates projected along the dendritic branch and computed the Pearson's correlation coefficient between their time-series activity during binocular viewing, excluding interstimulus intervals[81]. Only fields of view with 3 or more visually responsive spines were included in the analysis. To test for the statistical significance of correlation-distance relationship, we shuffled the correlations between the spine pairs in a field of view and binned these shuffled correlations by the original distance in 5 μm increments, repeating this shuffling 10,000 times to determine the 2.5% and 97.5% confidence intervals for each bin. To determine the size and number of functional clusters, we used graph theory to build a network representation of spines along a dendritic branch, and defined edges between pairs of spines that were within 5 μm of one another and had a pairwise correlation above their mean correlation to other spines in the field of view. A cluster was then defined as 2 or more spines comprising an isolated subnetwork.

Biophysical single neuron model

Biophysical model. To investigate the contributions of Hebbian and heterosynaptic plasticity in somatic orientation matching, we built a computational model of a single neuron in bV1 with two branches, each with N dendritic spines, to simulate synaptic plasticity. The initial values for the synaptic weights $w_k, k = 1, \ldots, N$ were drawn from the lognormal distribution with μ_w, σ_w. The interspine distance was drawn from the lognormal distribution with parameters μ_d, σ_d. Each synapse had a random eye preference drawn from the distribution experimentally-found at D1, and a direction preference θ_k. The initial direction preferences were assigned so that the soma's orientation preference in the contra and the ipsi viewing was mismatched. To simulate binocular visual experience over the critical period, we presented drifting grating stimuli with randomly switching directions θ_0[84]. The inputs were modeled as tuned Poisson spike trains, with average firing rate given by a von Mises distribution:

$$r_k = \left(\frac{A_k}{(1+\epsilon_k)} \frac{e^{z_k coscos(\theta_k - \theta_0)}}{2\pi I_0(z_k)} + \frac{A_k \epsilon_k}{(1+\epsilon_k)} \frac{e^{z_k coscos(\theta_k - \pi - \theta_0)}}{2\pi I_0(z_k)} \right). \quad (1)$$

In the equation above, $I_0(z_k)$ denotes the modified Bessel function of order 0, needed for normalization, A_k is the overall amplitude and ϵ_k is a random number between 0 and 1. When $\epsilon_k \to 0$, the tuning curve shows a peak at $\theta_0 = \theta_k$, indicating high direction selectivity, when $\epsilon_k \to 1$, the tuning curve shows two peaks, at $\theta_0 = \theta_k$ and at $\theta_0 = \theta_k - \pi$, indicating low direction selectivity. The term z_k in the Bessel function determines the width of the tuning curve, thus indicating the orientation selectivity. The variables A_k and z_k are initially drawn from a uniform distribution and change randomly whenever the direction of the stimuli changes (every 250 ms), following an Ornstein-Uhlenbeck distribution (see parameters in Supplementary Table 1).

Plasticity Induction. To induce plasticity, we first introduced a presynaptic accumulator ν_k and a postsynaptic accumulator u_k, inspired by a generalized model of heterosynaptic plasticity[51]. The presynaptic accumulator is a low-pass filtered version of the input spike train x_k:

$$\tau_\nu \dot{\nu}_k = -\nu_k(t) + \phi x_k(t). \quad (2)$$

The postsynaptic accumulator is a function of a weighted mean of the inputs onto the nearby synapses (heterosynaptic contribution), and the backpropagating action potential $B(t)$ (Hebbian contribution):

$$\tau_u \dot{u}_k = -u_k(t) + \sum_{l=1}^{N} s_{kl} w_l(t) x_l(t) + \tilde{s_k} B(t). \quad (3)$$

In the equation above, s_{kl} and $\tilde{s_k}$ are distance-dependent factors that decrease exponentially with the distance. In particular, $s_{kl} = e^{-\frac{d_{kl}^2}{2\sigma_s^2}}$ and $\tilde{s}_k = e^{-\frac{\tilde{d}_k^2}{2\sigma_{BAP}^2}}$, with d_{kl} $\left(\tilde{d_k}\right)$ denoting the distance of synapse k from the synapse l (from the soma), and σ_s (σ_{BAP}) being denoting the heterosynaptic factors. (Note that the distance factors affected the synapses along the same branch, but not synapses on two different branches). The variable $B(t)$ is binary (i.e., $B(t) = 1$ if a bAP is generated, $B(t) = 0$ otherwise). A bAP is generated whenever the somatic accumulator, defined as:

$$A(t) = \sum_{k=1}^{N} w_k(t) u_k(t), \quad (4)$$

reaches a threshold $A_{th}(t)$. The threshold increases whenever the soma generates a bAP, and decays exponentially otherwise.

The synaptic weight evolved on a slower timescale, as a function of the pre- and postsynaptic accumulators:

$$\tau_w \dot{w}_k = u_k(\nu_k - \rho), \quad (5)$$

where ρ represents the potentiation vs. depression threshold, i.e., when the input is strong enough such that $\nu_k(t)$ is larger than the threshold ρ, then the synaptic weight is strengthened, and the synaptic weight is weakened otherwise. The values for the synaptic weights were constrained in the range $[w_{\min}, w_{\max}]$. If the synaptic weight reached a value below $w_{\min}$, then the synapse was removed and was replaced with a new synapse depending on a probability p_{new}. The synaptic weight, as well as the eye and direction preferences, were chosen randomly for the new formed synapses. The parameters chosen for this model are listed in Supplementary Table 1.

Synaptic dynamics and clustering analysis. For the analysis of the relationship between spine activity and survival time, the normalized spine activity was defined as the integral of its presynaptic accumulator over time, divided by the maximal integral across spines. We measured survival time (taken as the fraction of time survived over total simulation time) only for spines present at the start of the simulation. The correlation with the soma was quantified by the Pearson correlation coefficient between the spine presynaptic accumulator and the somatic accumulator. The spine pair correlation vs. distance was quantified by the Pearson correlation coefficient between the presynaptic accumulators. To determine the size and number of clusters, we followed the same procedure as for the experimental data, namely we used graph theory to build a network representation of spines along a dendritic branch, and defined a cluster as any spine that was within 5 μm from another spine and had a pairwise correlation above the mean pairwise correlation.

Somatic interocular alignment. To quantify the somatic alignment during a testing phase, we measured the somatic activity (firing rate) for each direction, in the three different types of viewing (ipsi, contra, binocular). For each type of viewing, we defined the direction selectivity as $\widetilde{L} = \frac{\sum_k A(\theta_k) exp(i\theta_k)}{\sum_k A(\theta_k)}$, and the preferred direction of the grating as the arctangent of the imaginary and real component of vector $\widetilde{L}$. To measure the somatic mismatch, we normalized the somatic activity for each type of viewing and then calculated their absolute difference.

Quantification and statistical analysis

The statistical tests used in each analysis are indicated in the figure legends and main text. For most analysis, we used a two-tailed nonparametric statistical analysis (i.e. Wilcoxon's signed-rank test, Wilcoxon's rank sum test, and Kruskal-Wallis test) or from a shuffled distribution that was repeated10,000 times. In some cases where we had to test multiple conditions, we used a two-way ANOVA or a one-way ANOVA corrected for multiple comparison's using Tukey's post hoc correction. All statistical tests were done using MATLAB.

Reporting summary

Further information on research design is available in the Nature Portfolio Reporting Summary linked to this article.

Data availability

The processed data used to reproduce the figures in the manuscript are available on FigShare under the accession code (https://doi.org/10.6084/m9.figshare.28738592)[85]. Source data are provided with this paper.

Code availability

All code used to process the data and reproduce the figures in the manuscript have been uploaded on GitHub under the accession code (https://doi.org/10.5281/zenodo.15475970)[86].

References

1. Espinosa, J. S. & Stryker, M. P. Development and Plasticity of the Primary Visual Cortex. *Neuron* **75**, 230–249 (2012).
2. Cang, J. et al. Development of precise maps in visual cortex requires patterned spontaneous activity in the retina. *Neuron* **48**, 797–809 (2005).
3. Cang, J. et al. Selective disruption of one cartesian axis of cortical maps and receptive fields by deficiency in Ephrin-As and structured activity. *Neuron* **57**, 511–523 (2008).
4. O'Leary, D. D. M., Chou, S. J. & Sahara, S. Area patterning of the mammalian cortex. *Neuron* **56**, 252–269 (2007).
5. Ko, H. et al. The emergence of functional microcircuits in visual cortex. *Nature* **496**, 96–100 (2013).
6. Hoy, J. L. & Niell, C. M. Layer-specific refinement of visual cortex function after eye opening in the awake mouse. *J. Neurosci.* **35**, 3370–3383 (2015).
7. Jenks, K. R. & Shepherd, J. D. Experience-Dependent Development and Maintenance of Binocular Neurons in the Mouse Visual Cortex. *Cell Rep* **30**, 1982–1994.e4 (2020).
8. Tan, L., Ringach, D. L., Zipursky, S. L. & Trachtenberg, J. T. Vision is required for the formation of binocular neurons prior to the classical critical period. *Curr. Biol.* **31**, 4305–4313.e5 (2021).
9. Katz, L. C. & Shatz, C. J. Synaptic Activity and the Construction of Cortical Circuits. *Science (80-.)* **274**, 1133 LP–1131138 (1996).
10. Sur, M. & Rubenstein, J. L. R. Patterning and Plasticity of the Cerebral Cortex. *Science (80-.)* **310**, 805–810 (2005).
11. Levelt, C. N. & Hübener, M. Critical-Period Plasticity in the Visual Cortex. *Annu. Rev. Neurosci.* **35**, 309–330 (2012).
12. Wiesel, T. N. & Hubel, D. H. Single-Cell Responses in Striate Cortex of Kittens Desprived of Vision in One Eye. (1963).
13. Gordon, J. A. & Stryker, M. P. Experience-dependent plasticity of binocular responses in the primary visual cortex of the mouse. *J. Neurosci.* **16**, 3274–3286 (1996).
14. Frenkel, M. Y. & Bear, M. F. How monocular deprivation shifts ocular dominance in visual cortex of young mice. *Neuron* **44**, 917–923 (2004).
15. Antonini, A. & Stryker, M. P. Rapid Remodeling of Axonal Arbors in the Visual Cortex. *Science (80-.)* **260**, 1819–1821 (1993).
16. Majdan, M. & Shatz, C. J. Effects of visual experience on activity-dependent gene regulation in cortex. *Nat. Neurosci.* **9**, 650–659 (2006).
17. Tropea, D. et al. Gene expression changes and molecular pathways mediating activity-dependent plasticity in visual cortex. *Nat. Neurosci.* **9**, 660–668 (2006).
18. Lyckman, A. W. et al. Gene expression patterns in visual cortex during the critical period: Synaptic stabilization and reversal by visual deprivation. *Proc. Natl. Acad. Sci. USA.* **105**, 9409–9414 (2008).
19. Majewska, A. & Sur, M. Motility of dendritic spines in visual cortex in vivo: Changes during the critical period and effects of visual deprivation. *Proc. Natl. Acad. Sci. USA.* **100**, 16024–16029 (2003).
20. Oray, S., Majewska, A. & Sur, M. Dendritic spine dynamics are regulated by monocular deprivation and extracellular matrix degradation. *Neuron* **44**, 1021–1030 (2004).
21. Tropea, D., Majewska, A. K., Garcia, R. & Sur, M. Structural dynamics of synapses in vivo correlate with functional changes during experience-dependent plasticity in visual cortex. *J. Neurosci.* **30**, 11086–11095 (2010).

22. Yu, H., Majewska, A. K. & Sur, M. Rapid experience-dependent plasticity of synapse function and structure in ferret visual cortex in vivo. *Proc. Natl. Acad. Sci.* **108**, 21235 LP–21221240 (2011).
23. Zhou, Y., Lai, B. & Gan, W. B. Monocular deprivation induces dendritic spine elimination in the developing mouse visual cortex. *Sci. Rep.* **7**, 1–11 (2017).
24. Sun, Y. J. et al. Experience-dependent structural plasticity at pre- and postsynaptic sites of layer 2/3 cells in developing visual cortex. *Proc. Natl. Acad. Sci.* **116**, 21812 LP–21821820 (2019).
25. Wang, B. S., Sarnaik, R. & Cang, J. Critical Period Plasticity Matches Binocular Orientation Preference in the Visual Cortex. *Neuron* **65**, 246–256 (2010).
26. Sarnaik, R., Wang, B. S. & Cang, J. Experience-dependent and independent binocular correspondence of receptive field subregions in mouse visual cortex. *Cereb. Cortex* **24**, 1658–1670 (2014).
27. Gu, Y. & Cang, J. Binocular matching of thalamocortical and intracortical circuits in the mouse visual cortex. *Elife* **5** e22032 (2016).
28. Tan, L., Tring, E., Ringach, D. L., Zipursky, S. L. & Trachtenberg, J. T. Vision Changes the Cellular Composition of Binocular Circuitry during the Critical Period. *Neuron* **108**, 735–747.e6 (2020).
29. Tan, L., Ringach, D. L. & Trachtenberg, J. T. The Development of Receptive Field Tuning Properties in Mouse Binocular Primary Visual Cortex. *J. Neurosci.* **42**, 3546–3556 (2022).
30. Grutzendler, J., Kasthuri, N. & Gan, W. B. Long-term dendritic spine stability in the adult cortex. *Nature* **420**, 812–816 (2002).
31. Miller, K. D., Abbott, L. F. & Song, S. Competitive Hebbian learning through spike-timing-dependent synaptic plasticity. *Nat. Neurosci.* **3**, 919–926 (2000).
32. Jenks, K. R., Tsimring, K., Ip, J. P. K., Zepeda, J. & Sur, M. Heterosynaptic Plasticity and the Experience-Dependent Refinement of Developing Neuronal Circuits. *Front. Neural Circuits* **15**, 1–20 (2021).
33. Chater, T. E. & Goda, Y. My Neighbour Hetero — deconstructing the mechanisms underlying heterosynaptic plasticity. *Curr. Opin. Neurobiol.* **67**, 106–114 (2021).
34. Matsuzaki, M., Honkura, N., Ellis-Davies, G. C. R. & Kasai, H. Structural basis of long-termpotentiation in single dendriticspines. *Nature* **429**, 758–761 (2004).
35. Harvey, C. D. & Svoboda, K. Locally dynamic synaptic learning rules in pyramidal neuron dendrites. *Nature* **450**, 1195–1200 (2007).
36. Zhang, Y., Cudmore, R. H., Lin, D. T., Linden, D. J. & Huganir, R. L. Visualization of NMDA receptor - Dependent AMPA receptor synaptic plasticity in vivo. *Nat. Neurosci.* **18**, 402–409 (2015).
37. Kornijcuk, V., Kim, D., Kim, G. & Jeong, D. S. Simplified calcium signaling cascade for synaptic plasticity. *Neural Networks* **123**, 38–51 (2020).
38. Tazerart, S., Mitchell, D. E., Miranda-Rottmann, S. & Araya, R. A spike-timing-dependent plasticity rule for dendritic spines. *Nat. Commun.* **11** 4276 (2020).
39. Noguchi, J. et al. In vivo two-photon uncaging of glutamate revealing the structure-function relationships of dendritic spines in the neocortex of adult mice. *J. Physiol.* **589**, 2447–2457 (2011).
40. Hill, T. C. & Zito, K. LTP-induced long-term stabilization of individual nascent dendritic spines. *J. Neurosci.* **33**, 678–686 (2013).
41. Winnubst, J., Cheyne, J. E., Niculescu, D. & Lohmann, C. Spontaneous Activity Drives Local Synaptic Plasticity InVivo. *Neuron* **87**, 399–410 (2015).
42. Leighton, A. H., Cheyne, J. E. & Lohmann, C. Clustered synapses develop in distinct dendritic domains in visual cortex before eye opening. *Elife* **12**, 1–39 (2024).
43. Hedrick, N. G. et al. Learning binds new inputs into functional synaptic clusters via spinogenesis. *Nat. Neurosci.* **25**, 726–737 (2022).
44. El-Boustani, S. et al. Locally coordinated synaptic plasticity of visual cortex neurons in vivo. *Science.* **360**, 1340–1354 (2018).
45. Lee, K. F. H. H., Soares, C., Thivierge, J. P. & Béïque, J. C. Correlated Synaptic Inputs Drive Dendritic Calcium Amplification and Cooperative Plasticity during Clustered Synapse Development. *Neuron* **89**, 784–799 (2016).
46. Ujfalussy, B. B. & Makara, J. K. Impact of functional synapse clusters on neuronal response selectivity. *Nat. Commun.* **11**, 1–14 (2020).
47. Wilson, D. E., Whitney, D. E., Scholl, B. & Fitzpatrick, D. Orientation selectivity and the functional clustering of synaptic inputs in primary visual cortex. *Nat. Neurosci.* **19**, 1003–1009 (2016).
48. Polsky, A., Mel, B. W. & Schiller, J. Computational subunits in thin dendrites of pyramidal cells. *Nat. Neurosci.* **7**, 621–627 (2004).
49. Smith, S. L., Smith, I. T., Branco, T. & Häusser, M. Dendritic spikes enhance stimulus selectivity in cortical neurons in vivo. *Nature* **503**, 115–120 (2013).
50. Hiratani, N. & Fukai, T. Detailed dendritic excitatory/inhibitory balance through heterosynaptic spike-timing-dependent plasticity. *J. Neurosci.* **37**, 12106–12122 (2017).
51. Kirchner, J. H. & Gjorgjieva, J. Emergence of local and global synaptic organization on cortical dendrites. *Nat. Commun.* **12** 4005 (2021).
52. Hedrick, N. G. et al. Rho GTPase complementation underlies BDNF-dependent homo- and heterosynaptic plasticity. *Nature* **538**, 104–108 (2016).
53. Niculescu, D. et al. A BDNF-Mediated Push-Pull Plasticity Mechanism for Synaptic Clustering. *Cell Rep* **24**, 2063–2074 (2018).
54. Wang, B. S., Feng, L., Liu, M., Liu, X. & Cang, J. Environmental Enrichment Rescues Binocular Matching of Orientation Preference in Mice that Have a Precocious Critical Period. *Neuron* **80**, 198–209 (2013).
55. Holtmaat, A. J. G. D. et al. Transient and persistent dendritic spines in the neocortex in vivo. *Neuron* **45**, 279–291 (2005).
56. Majewska, A. K., Newton, J. R. & Sur, M. Remodeling of synaptic structure in sensory cortical areas In Vivo. *J. Neurosci.* **26**, 3021–3029 (2006).
57. Chen, M., Qi, J., Poo, M. & Yang, Y. Stability and dynamics of dendritic spines in macaque prefrontal cortex. *Natl. Sci. Rev.* **9** nwac125 (2022).
58. Xu, T. et al. Rapid formation and selective stabilization of synapses for enduring motor memories. *Nature* **462**, 915–919 (2009).
59. Trachtenberg, J. T. et al. Long-term in vivo imaging of experience-dependent synaptic plasticity in adult cortex. *Nature* **420**, 788–794 (2002).
60. Sjöström, P. J. & Nelson, S. B. Spike timing, calcium signals and synaptic plasticity. *Curr. Opin. Neurobiol.* **12**, 305–314 (2002).
61. Smith, S. L. & Trachtenberg, J. T. Experience-dependent binocular competition in the visual cortex begins at eye opening. *Nat. Neurosci.* **10**, 370–375 (2007).
62. Faguet, J., Maranhao, B., Smith, S. L. & Trachtenberg, J. T. Ipsilateral eye cortical maps are uniquely sensitive to binocular plasticity. *J. Neurophysiol.* **101**, 855–861 (2009).
63. Osako, Y. et al. Contribution of non-sensory neurons in visual cortical areas to visually guided decisions in the rat. *Curr. Biol.* **31**, 2757–2769.e6 (2021).
64. Niell, C. M. & Stryker, M. P. Modulation of Visual Responses by Behavioral State in Mouse Visual Cortex. *Neuron* **65**, 472–479 (2010).
65. Avitan, L. & Stringer, C. Not so spontaneous: Multi-dimensional representations of behaviors and context in sensory areas. *Neuron* **110**, 3064–3075 (2022).
66. Stringer, C. et al. Spontaneous behaviors drive multidimensional, brainwide activity. *Science.* **364** 255 (2019).
67. de Vries, S. E. J. et al. A large-scale, standardized physiological survey reveals functional organization of the mouse visual cortex. *Nat. Neurosci.* **23** 138–151 (2019).

68. Ko, H. et al. Functional specificity of local synaptic connections in neocortical networks. *Nature* **473**, 87–91 (2011).
69. Lee, W. C. A. et al. Anatomy and function of an excitatory network in the visual cortex. *Nature* **532**, 370–374 (2016).
70. Cossell, L. et al. Functional organization of excitatory synaptic strength in primary visual cortex. *Nature* **518**, 399–403 (2015).
71. Ding, Z. *et al*. Functional connectomics reveals general wiring rule in mouse visual cortex. *bioRxiv* 2023.03.13.531369 (2023).
72. Ko, H., Mrsic-Flogel, T. D. & Hofer, S. B. Emergence of Feature-Specific Connectivity in Cortical Microcircuits in the Absence of Visual Experience. *J. Neurosci.* **34**, 9812–9816 (2014).
73. Balcioglu, A. et al. Mapping thalamic innervation to individual L2/3 pyramidal neurons and modeling their 'readout' of visual input. *Nat. Neurosci.* **26**, 470–480 (2023).
74. Bauer, J. et al. Limited functional convergence of eye-specific inputs in the retinogeniculate pathway of the mouse. *Neuron* **109**, 2457–2468.e12 (2021).
75. Iacaruso, M. F., Gasler, I. T. & Hofer, S. B. Synaptic organization of visual space in primary visual cortex. *Nature* **547**, 449–452 (2017).
76. Scholl, B., Wilson, D. E. & Fitzpatrick, D. Local Order within Global Disorder: Synaptic Architecture of Visual Space. *Neuron* **96**, 1127–1138.e4 (2017).
77. Lee, K. S., Vandemark, K., Mezey, D., Shultz, N. & Fitzpatrick, D. Functional Synaptic Architecture of Callosal Inputs in Mouse Primary Visual Cortex. *Neuron* **101**, 421–428.e5 (2019).
78. Dorkenwald, S. et al. Binary and analog variation of synapses between cortical pyramidal neurons. *Elife* **11**, 1–26 (2022).
79. Holtmaat, A. et al. Long-term, high-resolution imaging in the mouse neocortex through a chronic cranial window. *Nat. Protoc.* **4**, 1128–1144 (2009).
80. Chen, T.-W. et al. Ultrasensitive fluorescent proteins for imaging neuronal activity. *Nature* **499**, 295–300 (2013).
81. Scholl, B., Thomas, C. I., Ryan, M. A., Kamasawa, N. & Fitzpatrick, D. Cortical response selectivity derives from strength in numbers of synapses. *Nature* **590**, 111–114 (2021).
82. Scholl, B. et al. A binocular synaptic network supports interocular response alignment in visual cortical neurons. *Neuron* **110**, 1573–1584.e4 (2022).
83. Mazurek, M., Kager, M. & Van Hooser, S. D. Robust quantification of orientation selectivity and direction selectivity. *Front. Neural Circuits* **8**, 1–17 (2014).
84. Xu, X., Cang, J. & Riecke, H. Development and binocular matching of orientation selectivity in visual cortex: A computational model. *J. Neurophysiol.* **123**, 1305–1319 (2020).
85. Tsimring, K. et al. Large-scale synaptic dynamics drive the reconstruction of binocular circuits in mouse visual cortex. *FigShare*. https://doi.org/10.6084/m9.figshare.28738592 (2025).
86. Tsimring, K. et al. Large-scale synaptic dynamics drive the reconstruction of binocular circuits in mouse visual cortex. *GitHub*. https://doi.org/10.5281/zenodo.15475970 (2025).

Acknowledgements

This work was supported by NIH grants R01MH126351 (M.S.), R01EY028219 (M.S.), the Picower Institute Innovation Fund (M.S.), F31EY033649 (K.T.), F32EY032756 (K.J.), Hong Kong RGC Early Career Scheme 24117220 (J.I.), and Marie Skłodowska Curie Innovative Training Network SmartNets 860949 (C.C.).The authors thank Emma Odom, José C. Zepeda, and members of the Sur lab for scientific discussions, help, and support.

Author contributions

This project was conceptualized by M.S., K.T., K.J., and J.I. All two-photon imaging, data processing, and analysis was performed by K.T., with input from G.H. and K.J. Computational modeling was done by C.C., with input from J.G. K.T. wrote the manuscript with input from M.S. and K.J. All authors edited the manuscript.

Competing interests

The authors declare no competing interests.

Additional information

Supplementary information The online version contains supplementary material available at https://doi.org/10.1038/s41467-025-60825-y.

Correspondence and requests for materials should be addressed to Mriganka Sur.

Peer review information *Nature Communications* thanks the anonymous reviewer(s) for their contribution to the peer review of this work. A peer review file is available.